Excitation-autoionization through $3d$-$4l$ inner-shell excitations in Cu- to Kr-like ions and the effect on fractional-ion-abundance balance in coronal plasmas

D. Mitnik, P. Mandelbaum, and J. L. Schwob
Racah Institute of Physics, The Hebrew University, 91904 Jerusalem, Israel

A. Bar-Shalom and J. Oreg
Nuclear Research Center–Negev, P.O. Box 9001, 84190 Beer Sheva, Israel

W. H. Goldstein
Lawrence Livermore National Laboratory, P.O. Box 808, Livermore, California 94550

(Received 15 February 1994; revised manuscript received 11 July 1994)

Excitation of inner-shell electrons into autoionizing levels followed by autoionization (EA) can enhance the total ionization rate. For ions isoelectronic to elements of the fourth row, the present results show that the enhancements can be much more important than those previously calculated for the preceding isoelectronic sequences. $\Delta n=1$ $3d$-$4l$ inner-shell excitations, which are the dominant EA channels, are considered here. Detailed computations of EA rates were performed using the relativistic distorted-wave method, and the behavior of the EA rate coefficients along the Cu, Zn, Ga, and Kr isoelectronic sequences has been analyzed. In the other sequences from Ge to Br with configurations involving a very large number of levels, EA calculations have been performed for a few elements only. In view of an easy use of the data, and for application to other elements, approximate analytical expressions have been deduced for ionization energies, average inner-shell excited-configuration energies, total electron-impact excitation rates, as well as average branching ratios for autoionization. These data enable a direct evaluation of the EA rates in all the sequences from Cu to Kr for all the elements with $40\leq Z\leq 92$. Finally, the EA rate coefficients were introduced in the coronal ionization rate equations. Fractional ion abundances for Mo ($Z=42$), Xe ($Z=54$), Pr ($Z=59$), and Dy ($Z=66$) obtained with and without taking into account EA processes are presented. The results show a decrease of up to 40% in the temperature of maximum abundance for Kr- to Ni-like ions.

PACS number(s): 32.80.Dz, 34.80.Dp, 34.80.Kw, 52.25.Kn

I. INTRODUCTION

Excitation of inner-shell electrons into highly excited autoionizing levels followed by autoionization is an important process which can significantly enhance the total ionization rate. This excitation-autoionization (EA) process has been studied mainly for ions belonging to sequences isoelectronic to light elements having simple ground-state structure. In particular, several works have been performed for ions of the Li and Na isoelectronic sequences [1–4]. In these sequences, it was found that direct ionization could be enhanced by up to a factor of 2 or 3 by including EA processes. Calculations for the above sequences have been used in the prediction of fractional ion abundance of elements found in astrophysical plasma [5,6]. However, very few EA calculations have been performed for heavier ionized atoms belonging to the sequences isoelectronic to the fourth row elements [7]. This is quite surprising, since it has been pointed out by Cowan and Mann [8] that the Cu (ground $3d^{10}4s$), Zn (ground $3d^{10}4s^2$), and Ga (ground $3d^{10}4s^24p$) sequences are, with ten $3d$ inner-shell electrons and only a few $4l$ outer electrons, very good candidates for EA processes. This may be understood in light of the lack of rapid and efficient methods for computing electron-impact excitation rates, which permit one to undertake the relatively complex task of calculating rates for these sequences with a very large number of levels. Such methods have been developed only recently. Thus some computations have been performed recently for a few elements in the Ga isoelectronic sequence [9,10] and for the Zn-like molybdenum ion [11]. These first computations have shown that EA processes through $3d$-$4l$ electron-impact excitations could enhance the total ionization rate coefficient by up to a factor of 4 at an electron temperature T_e equal to the ionization energy. Moreover, for these sequences the first ionization limit lies in the middle of those configurations which can be excited through $3d$-$4l$ inner-shell electron-impact excitations from the ground state. Due to the progressive decrease of the inner-shell excited configuration energies below the first ionization limit as Z increases, one expects sharp discontinuities in the EA effect along an isoelectronic sequence. This effect is due to the closing of autoionization channels as the energy of a configuration falls below the ionization limit. These discontinuities in the EA rates are unlike the behavior of the EA effect in sequences like that of Li or Na, where the inner-shell excited configurations lie well above the ionization limit, and thus the change in EA rates is dictated mostly by the smooth change of the radiative decays compared to the autoionization rates.

The present work represents the results of extensive

calculations of EA rates through $3d$-$4l$ inner-shell excitations from the ground state for ionized heavy elements ($40 \leq Z \leq 92$) along the sequences which are isoelectronic to the elements of the fourth row. The inner-shell excitations considered here are the $\Delta n = 1$ $3d$-$4l$ transitions which are expected to give the most important EA effect. The lack of smooth behavior along each isoelectronic sequence necessitates detailed *level-by-level* EA calculations for each element. These calculations are performed over a wide range of electron temperature. The results of these computations can then be used to compute the EA effect on the fractional ion abundances at coronal equilibrium [12]. First, in Sec. II, the theoretical methods are described briefly. In Sec. III, the results of average energy computations of the relevant inner-shell configurations are discussed. This gives a general insight into the peculiar behavior of EA along the isoelectronic sequences. The results of the detailed EA rate computation for the Cu, Zn, Ga, and Kr isoelectronic sequences are given in Sec. IV. For other sequences, detailed calculations have been performed for only a few elements. Section V shows how these results can be summarized in simple analytical formulas for all the elements as a function of T_e. This permits the easy introduction of the results in the coronal ionization model. Finally, results of fractional ion abundance calculations with and without taking into account the EA processes are presented in Sec. VI for the elements Mo, Xe, Pr, and Dy. The importance of EA processes, especially at the relevant electron temperatures around the maximum ion abundance, is analyzed.

II. THEORETICAL AND CALCULATIONAL METHODS

The theoretical approach is basically the same as that used in our previous work [10]. A more complete description of the theory can be found in Ref. [13]. The theory is implemented in the computer package HULLAC, which calculates atomic many-electron relativistic wave functions, energies, radiative transition probabilities, and distorted-wave (DW) autoionization (electron capture) rates and collisional excitation cross sections. In this package, the RELAC code [14] calculates the bound, mixed configuration states, energies, and transition probabilities using the relativistic parametric potential method [14,15], which minimizes the first-order energy of any desired state or configuration average. In our calculations the potential is optimized separately for the ground and excited configurations for each ionization stage. Recently, the RELAC code was extended to calculate DW autoionization rates as well [11]. The CROSS code calculates the DW cross sections for electron-impact excitations using the "factorization-interpolation" method [13].

The results presented here for the sequences considered (Cu to Kr) are limited to elements with $Z \geq 40$, since for low ionization stages the RELAC calculation method becomes less accurate.

The total rate coefficient S^{EA} for excitation-autoionization from a level g of the ground configuration $3d^{10}4s^m4p^n$ of an ion of charge r to all levels k of the next ion $r+1$, through inner-shell excitation to any autoionizing level j of the $3d^94s^m4p^n4d$ or $3d^94s^m4p^n4f$ intermediate configuration of ion r, is given by

$$S^{\mathrm{EA}} = \sum_j \left[\frac{Q_{gj} \sum_k A^a_{jk}}{\sum_i A_{ji} + \sum_k A^a_{jk}} \right] \equiv \sum_j Q_{gj} B^a_j , \qquad (1)$$

where Q_{gj} is the electron-impact excitation rate coefficient from the ground level g to level j of the intermediate configuration. A^a_{jk} is the autoionization rate coefficient from level j to a level k of the next ion. A_{ji} is the Einstein spontaneous radiative coefficient from level j to a lower level i of the same ion. B^a_j is the branching ratio for autoionization from the autoionizing level j.

III. AVERAGE ENERGIES OF INNER-SHELL EXCITED CONFIGURATIONS

The best way to get a general insight into the very peculiar behavior of the excitation-autoionization effect along the different isoelectronic sequences, prior to performing detailed EA computations, is to look at the average energies of the inner-shell excited configurations that are excited from the ground level of the parent ion. Thus the statistically weighted average energies of the configurations excited through $3d$-$4d$ and $3d$-$4f$ electron-impact excitation and the first ionization energy are computed for each ion using the RELAC code. Figure 1 shows the ratio between the average energy of the inner-shell excited configuration $3d^94s^m4p^n4d$ and the first ionization energy E_I as a function of Z for the eight consecutive isoelectronic sequences: from the Cu ($3d^94s4d$) to the Kr ($3d^94s^24p^64d$) sequences. For each sequence, at relatively low Z this ratio is higher than unity, and thus the ion excited to a level inside these configurations can eventually autoionize. For higher Z

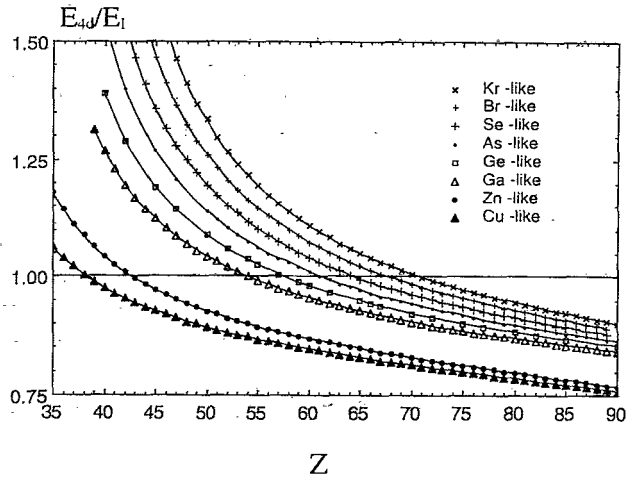

FIG. 1. Ratio between the average transition energy for inner-shell excitation from $3d^{10}4s^m4p^n$ to $3d^94s^m4p^n4d$ configuration, and the first ionization energy E_I, as a function of Z in the Cu ($m=1, n=0$) to Kr ($m=2, n=6$) isoelectronic sequences.

the ratio decreases, becoming eventually lower than unity, leading to the closing of autoionization channels. As can be observed from Fig. 1, the value of Z at which the ratio equals one varies in the different isoelectronic sequences, from about $Z=38$ in the Cu sequence to $Z=71$ in the Kr sequence. Thus the number of ionization stages of an element in which the $3d$-$4d$ excitation can lead to EA processes varies from element to element. From this simple picture, one can expect drastic changes in the EA contribution to the total ionization rate as a function of Z. Similar behavior is observed for $3d$-$4f$ inner-shell excitations, as shown in Fig. 2. The general trend is the same except for a shift of the curves towards higher Z because of the higher $3d$-$4f$ excitation energies.

It must be stressed that the picture given by the average configuration energies is only a rough one. Indeed, in most of the cases the excited configurations contain a large number of levels, which are spread out around the center of gravity of the configurations. Configuration interaction can scatter the level energies even farther from the configuration average values. Thus the crossing of the inner-shell excited configuration with the ionization limit as Z increases occurs in reality over a somewhat extended Z range, rather than at a precise Z value as predicted from the curves of Figs. 1 and 2. Moreover, in several cases, the total collisional excitation from the ground state to the particular configurations is due mostly to only a few inner-shell excited levels, which have energy values that might be quite different from the statistical weighted average energy. Consequently, the *effective* crossing between the inner-shell excited configuration energies and the ionization limit may take place at Z values slightly different than those predicted from the average energy curves.

Nevertheless, the average energies are useful for giving an approximate prediction for which ions the EA processes can be important. Also, it shows that one has to expect important irregularities of the EA processes along the different isoelectronic sequences. These general predictions were confirmed by detailed EA calculations as presented in the next section. Finally, the average energy calculations will be used in the analytical expressions for the total collisional excitation rates, needed for the general approximate EA treatment (Sec. V).

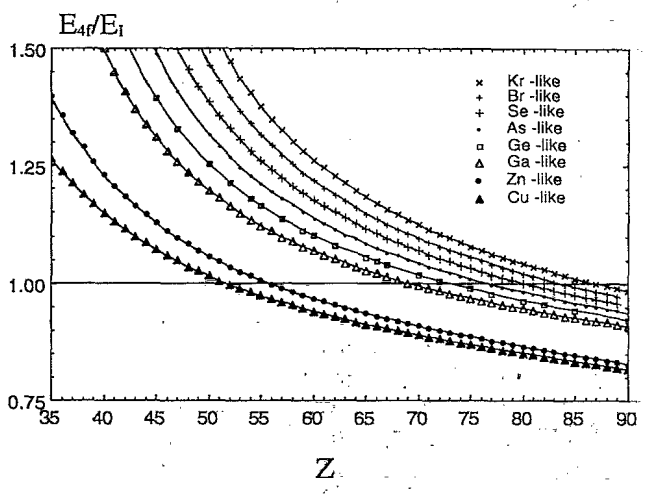

FIG. 2. Ratio between the average transition energy for inner-shell excitation from $3d^{10}4s^m4p^n$ to $3d^94s^m4p^n4f$ configuration, and the first ionization energy E_I, as a function of Z in the Cu ($m=1,n=0$) to Kr ($m=2,n=6$) isoelectronic sequences.

IV. DETAILED EA RATE COEFFICIENT CALCULATIONS

A. S^{EA} and ionization enhancement factor calculations

The rate coefficients S^{EA} for excitation-autoionization through $\Delta n=1$ $3d$-$4l$ inner-shell excitations are calculated using the detailed multiconfiguration computations for every element with $40\leq Z\leq 92$ along the Cu, Zn, Ga, and Kr isoelectronic sequences. A few errors found in Ga-like ion results previously published [10] have been corrected here. The calculations are performed in the electron temperature range $0.1E_I\leq kT_e\leq 2E_I$, where E_I is the first ionization limit of each ion. For a check, the results of the method used here are compared with published data for the B and Ne isoelectronic sequences [16,17]. The comparison shows good agreement between the different methods.

In the present calculations the effect of configuration mixing is included. Basically, the mixing may have three main effects in the EA computations. The first is a change in the energy of the levels; this can produce drastic changes in the autoionization rates for those ions having levels very close to the ionization limit. The second effect is the opening of new allowed radiative decay channels; this reduces the branching ratios for autoionization. Finally, configuration mixing redistributes the level-to-level excitation rates and may significantly affect the total EA rates.

A detailed account of the full computations for the individual level contributions, including the effects of configuration mixing and the comparison with the published data for other sequences, is beyond the scope of this paper and will be presented elsewhere. In the present work, only the final results reflecting the total EA effect for entire configurations through $3d$-$4l$ electron-impact excitations are presented.

In order to evaluate the effective enhancement of the collisional ionization rate coefficients due to the EA processes, an enhancement factor R is defined as follows:

$$R\equiv\frac{(S+S^{EA})}{S}, \tag{2}$$

where S is the direct collisional ionization rate coefficient.

Codes for calculating quantum-mechanical ionization rates with comparable accuracy to our collisional excitation rates are discussed, for instance, in Ref. [18]. In our previous work on the Ga isoelectronic sequence [10], a modified plane-wave Born approximation (PWBA) method, using the free-electron model, has been used for calculating direct collisional ionization rate coefficients. However, for simplicity we have used here the widely applied analytical Lotz formula [19]. A comparison between results using this formula and the PWBA calcula-

tions shows that the Lotz semiempirical approximation overestimates the rates. In the Ga sequence, the discrepancy varies from about 10% around $Z=45$ to a maximum of 22% for $Z=60$, at $kT_e=E_I$. Thus, in view of the large EA contribution expected here, the Lotz formula is sufficiently accurate, the enhancement factor being underestimated slightly. Moreover, this approximation is used in the ionization balance calculations (Sec. VI), and thus the choice of this formula allows a direct comparison with previous plasma modeling results using this approximation [20] but without EA.

The rate coefficient S_r for direct ionization (including inner-shell ionizations) of an ion of charge r in the ground state by electron impact is given according to the Lotz formula by

$$S_r=3.0\times10^{-6}\sum_s \frac{\zeta_s}{kT_e^{3/2}}\left\{\frac{E_1(E_{r,s}/kT_e)}{(E_{r,s}/kT_e)}\right\}, \qquad (3)$$

where S_r is given in $\mathrm{cm^3\,s^{-1}}$, kT_e is the electron temperature in eV, ζ_s is the electron occupancy number of the subshell s, and $E_{r,s}$ is the binding energy in eV of the electrons in this subshell. E_1 is the exponential integral function. The summation can be reduced to a few subshells which contribute significantly to direct ionization in Maxwellian electron distribution plasma. In the present detailed calculations the valence shell ($4s$ or $4p$) and the three next inner subshells ($3s$, $3p$, and $3d$, or $3p$, $3d$, and $4s$) are taken into consideration. The electron binding energies are given in Appendix A.

B. Cu isoelectronic sequence

The ground state of the ions belonging to this sequence is $3d^{10}4s$. The inner-shell collisional excitations in the S^{EA} calculation include excitations to all the levels of the $3d^9 4s4d$ and $3d^9 4s4f$ configurations, which can be populated by direct excitation from the ground state. In addition, the model includes the configurations that could produce configuration mixing effects [21]: $3d^9 4p^2$ (which mixes strongly with $3d^9 4s4d$) and $3d^9 4p4d$ (which mixes with $3d^9 4s4f$). It appears, though, that the introduction of $3d^9 4p^2$ mixing does not lead to any significant change in the EA final rates.

The radiative decays include transitions to the ground state, and the lower configurations $3d^{10}4l$ ($l=p,d,f$), as well as to the inner-shell excited configurations $3d^9 4s^2$ and $3d^9 4s4p$ (which lie below the first ionization limit for all the ions considered here). Radiative transitions between the autoionizing inner-shell excited configurations are also taken into account.

The autoionization processes considered here are to the ground state $3d^{10}$ of the Ni-like ions only, since the first excited Ni-like ion levels lie well above the Cu-like inner-shell excited levels. Secondary autoionization processes, i.e., those which might follow a primary radiative decay to a lower inner-shell excited configuration, are taken into account in the S^{EA} rate calculations neither in this sequence, nor in the Zn and Ga sequences. This simplification is justified since for low-Z elements the primary $\Delta n=0$ radiative decay channels are not important; whereas for high-Z elements these radiative transitions become significant; however, the relevant lower configurations ($3d^9 4s4p$, $3d^9 4s4d$) are no longer autoionizing.

The results of calculations for the total EA rates are given in Table I for $40\le Z\le 56$. For $Z\ge 56$, all the autoionizing channels considered here are closed, and $S^{EA}=0$. Figure 3 shows the ionization enhancement factor R [as defined in Eq. (2)] as a function of Z at three

TABLE I. Total rate coefficients S^{EA} for excitation-autoionization through $3d^{10}4s$-$3d^9 4s4d,4f$ inner-shell excitations, in the Cu isoelectronic sequence. The rates have been calculated in the electron temperature range from 0.3 to 2 times the first ionization energy E_I. $X[-Y]$ means $X\times10^{-Y}$. The coefficients are given in $\mathrm{cm^3\,s^{-1}}$ units.

Element	Z \ T_e	$0.3E_I$	$0.5E_I$	$0.7E_I$	$1.0E_I$	$2.0E_I$
Zr	40	1.63[−10]	5.78[−10]	9.59[−10]	1.36[−9]	1.93[−9]
Nb	41	1.50[−10]	5.26[−10]	8.69[−10]	1.23[−9]	1.74[−9]
Mo	42	1.43[−10]	4.94[−10]	8.10[−10]	1.14[−9]	1.61[−9]
Tc	43	1.36[−10]	4.61[−10]	7.50[−10]	1.05[−9]	1.47[−9]
Ru	44	1.27[−10]	4.22[−10]	6.81[−10]	9.49[−10]	1.31[−9]
Rh	45	5.92[−11]	2.10[−10]	3.51[−10]	5.06[−10]	7.53[−10]
Pd	46	4.93[−11]	1.71[−10]	2.83[−10]	4.05[−10]	5.94[−10]
Ag	47	4.42[−11]	1.51[−10]	2.47[−10]	3.51[−10]	5.10[−10]
Cd	48	4.20[−11]	1.41[−10]	2.29[−10]	3.24[−10]	4.67[−10]
In	49	3.99[−11]	1.32[−10]	2.13[−10]	3.00[−10]	4.30[−10]
Sn	50	3.76[−11]	1.23[−10]	1.98[−10]	2.77[−10]	3.95[−10]
Sb	51	3.44[−11]	1.11[−10]	1.79[−10]	2.51[−10]	3.58[−10]
Te	52	2.90[−11]	9.39[−11]	1.51[−10]	2.12[−10]	3.03[−10]
I	53	2.52[−11]	8.18[−11]	1.32[−10]	1.87[−10]	2.70[−10]
Xe	54	2.28[−11]	7.33[−11]	1.18[−10]	1.66[−10]	2.39[−10]
Cs	55	1.28[−11]	4.11[−11]	6.62[−11]	9.32[−11]	1.35[−10]
Ba	56	0	0	0	0	0

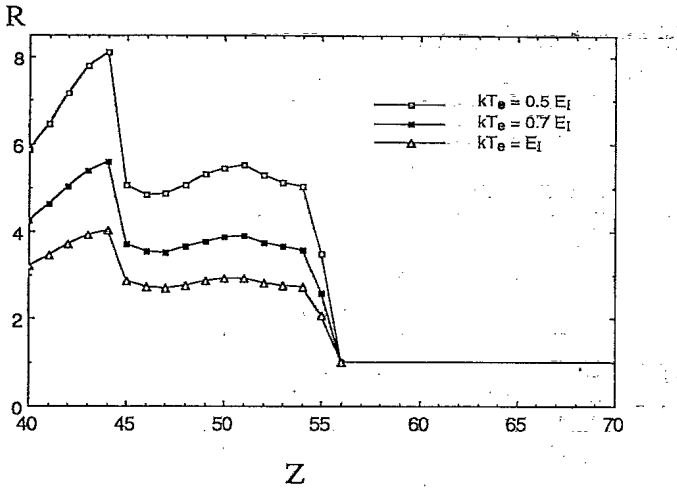

FIG. 3. Ratio R of total ionization rate coefficient ($S^{EA}+S$) to direct ionization rate coefficient S, at electron temperatures equal to 0.5, 0.7, and 1.0 times the first ionization energy E_I for each ion, as a function of Z, in the Cu isoelectronic sequence.

different electron temperatures corresponding to $kT_e=0.5$, 0.7, and 1.0 times the first ionization energy. At low Z, the autoionizing configurations $3d^9 4s 4d$ and $3d^9 4s 4f$ are relatively high with respect to the first ionization limit. For $40 \le Z \le 44$ the ratio R increases as a function of Z. This is due to the fact that the energies of the $3d^9 4s 4d$ and $3d^9 4s 4f$ levels are progressively decreasing as Z increases, thus favoring more and more the inner-shell excitation processes. The first abrupt decrease in R occurs at $Z=45$ and has a simple explanation: about 75% of the total excitation rate coefficients from the ground state to the $3d^9 4s 4d$ configuration is due to excitation to a single level, $3d^9_{5/2} 4s(3) 4d_{5/2}[J=\frac{1}{2}]$. This level, which is the highest in the configuration, falls below the ionization limit for all elements with Z greater than 44. Consequently, the effective closing of the $3d^9 4s 4d$ autoionization channels appears in this isoelectronic sequence at $Z=45$. This value of Z is slightly larger than predicted from the simple average energy curve in Fig. 1. The inner-shell transitions from the ground state to the $3d^9 4s 4f$ configuration are dominated by a few levels; therefore the successive closing of autoionization channels as Z further increases can also be observed in Fig. 3.

Another possible EA channel is through the inner-shell excited levels $3p^5 3d^{10} 4s 4l$. Calculations for this process are performed in this sequence only, for several elements, and show that the contribution of these channels leads to a limited effect (an enhancement of about 50% of the direct ionization rates, at $kT_e=E_I$). This is not negligible, but still small compared to the high enhancement value, R, due to $3d$-$4l$ excitations for low-Z ions. Thus, for elements with $Z \le 44$, neglecting the $3p$-$4l$ excitations leads to an underestimation of the total (direct plus EA) ionization rate by less than 10% (at a temperature of maximum ion abundance). However, for higher-Z elements for which $3d$-$4d$ EA channels are closed, and only $3d$-$4f$ EA processes remain, the underestimation reaches more than 20%. The relative $3p$-$4l$ EA effect is expected to decrease for the following sequences. This additional contribution is not included in the results presented in this work.

C. Zn isoelectronic sequence

The ground state in this sequence is $3d^{10} 4s^2$. The inner-shell excited configurations $3d^9 4s^2 4l$ ($l=p,d,f$), which are populated by collision from the ground state, are considered here. In fact $3d^9 4s^2 4p$ is autoionizing only for a few low-Z elements; moreover, the calculations show that its contribution to the total EA rate is not significant. The additional configurations introduced in the EA calculations to take into account the most important mixing are $3d^9 4s 4p^2$ (which mixes with $3d^9 4s^2 4d$) and $3d^9 4s 4p 4d$ (which mixes with $3d^9 4s^2 4f$). For the radiative transition decays, the $3d^{10} 4s 4p$ and $3d^{10} 4s 4d$ low-lying configurations are considered in addition to the ground state. Radiative transitions among the inner-shell excited configurations are also introduced. Finally, the present model includes the autoionization processes to the $3d^{10} 4s$, $3d^{10} 4p$, and $3d^{10} 4d$ levels of the next Cu-like ionization stage.

The results of the total EA rate coefficients are given in Table II for $40 \le Z \le 61$. For $Z \ge 61$ all the autoionizing channels considered here are closed, and $S^{EA}=0$. Figure 4 shows the ionization enhancement factor R as a function of Z at three electron temperatures corresponding to $kT_e=0.5$, 0.7, and 1.0 times the ionization energy. The general trend is the same as that observed in the Cu sequence. The first important decrease in the S^{EA} rate coefficient is observed at $Z=49$ and is due to the closing of the $3d^9 4s^2 4d$ autoionization channels.

In the Zn sequence, the effect of configuration mixing can be especially significant due to the fact that the ground state is a closed shell with $J=0$. In this case, without configuration interaction, the dominant $3d$-$4f$

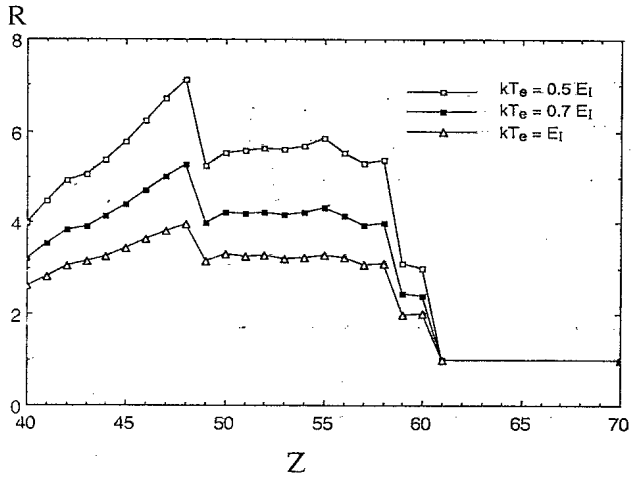

FIG. 4. Ratio R of total ionization rate coefficient ($S^{EA}+S$) to direct ionization rate coefficient S, at electron temperatures equal to 0.5, 0.7, and 1.0 times the first ionization energy E_1 for each ion, as a function of Z, in the Zn isoelectronic sequence.

TABLE II. Total rate coefficients S^{EA} for excitation-autoionization through $3d^{10}4s^2$-$3d^9 4s^2 4df,4f$ inner-shell excitations, in the Zn isoelectronic sequence. The rates have been calculated in the electron temperature range from 0.3 to 2 times the first ionization energy E_I. $X[-Y]$ means $X\times10^{-Y}$. The coefficients are given in $cm^3 s^{-1}$ units.

Element	Z \ T_e	$0.3E_I$	$0.5E_I$	$0.7E_I$	$1.0E_I$	$2.0E_I$
Zr	40	1.55[−10]	5.75[−10]	9.76[−10]	1.40[−9]	1.97[−9]
Nb	41	1.50[−10]	5.47[−10]	9.15[−10]	1.30[−9]	1.82[−9]
Mo	42	1.46[−10]	5.17[−10]	8.61[−10]	1.22[−9]	1.69[−9]
Tc	43	1.26[−10]	4.51[−10]	7.47[−10]	1.06[−9]	1.50[−9]
Ru	44	1.14[−10]	4.12[−10]	6.85[−10]	9.73[−10]	1.38[−9]
Rh	45	1.11[−10]	3.87[−10]	6.40[−10]	9.05[−10]	1.27[−9]
Pd	46	1.07[−10]	3.67[−10]	6.04[−10]	8.49[−10]	1.19[−9]
Ag	47	1.04[−10]	3.50[−10]	5.67[−10]	7.94[−10]	1.11[−9]
Cd	48	9.89[−11]	3.30[−10]	5.31[−10]	7.39[−10]	1.02[−9]
In	49	5.75[−11]	2.01[−10]	3.32[−10]	4.76[−10]	6.99[−10]
Sn	50	5.56[−11]	1.91[−10]	3.16[−10]	4.50[−10]	6.55[−10]
Sb	51	5.07[−11]	1.72[−10]	2.81[−10]	3.97[−10]	5.72[−10]
Te	52	4.69[−11]	1.56[−10]	2.54[−10]	3.58[−10]	5.13[−10]
I	53	4.27[−11]	1.40[−10]	2.26[−10]	3.17[−10]	4.50[−10]
Xe	54	3.93[−11]	1.29[−10]	2.06[−10]	2.88[−10]	4.08[−10]
Cs	55	3.77[−11]	1.21[−10]	1.93[−10]	2.68[−10]	3.78[−10]
Ba	56	3.17[−11]	1.03[−10]	1.67[−10]	2.35[−10]	3.38[−10]
La	57	2.77[−11]	8.90[−11]	1.43[−10]	2.00[−10]	2.86[−10]
Ce	58	2.57[−11]	8.26[−11]	1.33[−10]	1.88[−10]	2.70[−10]
Pr	59	1.17[−11]	3.69[−11]	5.88[−11]	8.17[−11]	1.17[−10]
Nd	60	1.01[−11]	3.23[−11]	5.18[−11]	7.27[−11]	1.04[−10]
Pm	61	0	0	0	0	0

transitions from the ground state involve only the $4f$ levels with $J=1$. In particular, for all the ions in the Z range relevant to EA processes ($Z\leq60$), about 80% of the total excitation rate to $3d^9 4s^2 4f$ is due to the level $3d^9_{3/2}4s^2 4f_{5/2}[J=1]$ (which is the highest energy level in the $3d^9 4s^2 4f$ configuration and corresponds to the $^1P_1$ level in LS coupling). Consequently, in this isolated configuration computation, the EA rate is very sensitive to the position of this single level versus ionization limit. For instance, for the Zn-like praseodymium ion ($Z=59$), only this level would have an energy slightly above the first ionization limit, but this level would lie below the ionization limit for the Zn-like ion neodymium ($Z=60$), causing a complete closing of autoionization channels. Thus the ionization enhancement factor R computed in this frame would have shown an abrupt decrease from $R=2.93$ at $Z=59$ to $R=1$ at $Z=60$ (for $kT_e=E_I$).

However, present calculations which take into account the interaction with the $3d^9 4s 4p 4d$ configuration, which is predicted to be important [21], show a quite different picture due to the fact that the excitation rate is now shared by many levels. Indeed, the distribution of the excitation rates now gives about 40% of the total rate for the highest energy level of the configuration $3d^9(4s^2 4f+4s4p4d)$, and about 30% for the next one. For the Zn-like cerium ion ($Z=58$), these two levels can autoionize, and the calculated enhancement factor is $R=3.12$. For the Pr ion, only the first level remains above the ionization limit, and therefore R drops to 2.00. Due to configuration mixing, this level is still above the ionization limit in the Nd ion, too, giving $R=1.97$. The final drop of R to unity occurs only in the Zn-like promethium ion ($Z=61$), as shown in Fig. 4. Thus the configuration mixing introduced in the present computations shifts the final decrease observed in the S^{EA} rate from $Z=60$ to $Z=61$. It should be noticed, however, that the accuracy of these particular theoretical predictions might be questioned, since the absolute precision of the computed energies is of the order of 0.5% only.

D. Ga isoelectronic sequence

The ground configuration of Ga-like ions is $3d^{10}4s^2 4p$. Since the EA computations will be applied here to the coronal regime in which only the lower level $3d^{10}4s^2 4p_{1/2}$ is significantly populated, EA from $3d^{10}4s^2 4p_{3/2}$ will not be presented in this work. The effect of EA processes through $3d$-$4l$ electron-impact inner-shell excitations for Ga-like ions has already been discussed for a few elements [9,10]. The inner-shell excited configurations considered here are $3d^9 4s^2 4p 4l$ ($l=p,d,f$). In fact, results of the calculations show that the contribution of the $3d^9 4s^2 4p^2$ configuration to the total S^{EA} coefficient is lower than 15% for Zr ($Z=40$), lower than 4% for Nb ($Z=41$), and lower than 0.15% for Mo ($Z=42$). Nevertheless, this contribution is taken into account in the present detailed calculations for the Ga sequence. However, the $3d\rightarrow4p$ excitation will not be included in calculations for the further sequences, for which the contribution is found to be completely negligible. The $3d^9 4s^2 4d^2$ configuration is included, since this leads to significant configuration mixing with $3d^9 4s^2 4p 4f$.

Besides the ground state, the $3d^{10}4s^24d$ and $3d^{10}4s^24f$ configurations are introduced for the radiative decays. Radiative transitions among the inner-shell excited configurations are also included. Autoionization processes to the Zn-like $3d^{10}4s^2$, $3d^{10}4s4p$, $3d^{10}4p^2$, and $3d^{10}4s4d$ configurations are taken into account. Table III shows the total rate coefficient S^{EA} for the elements with $40 \leq Z \leq 81$. For $Z \geq 81$ $S^{EA}=0$. Figure 5 displays the ionization enhancement ratio R as a function of Z at three electron temperatures (corresponding to $kT_e=0.5$, 0.7, and 1.0 times E_I). In the first Z range, $40 \leq Z \leq 58$, R is an increasing function of Z as observed in the previous sequences. The closing of EA channels through $3d^94s^24p4d$ occurs at $Z=59$ (Pr). For $Z>59$ one observes an almost continuous decrease in S^{EA} due to the successive closings of EA channels through the many levels of the $3d^94s^24p4f$ configuration. Another steep decrease appears at $Z=70$; in fact, the R factor does not drop completely to unity, due to the fact that a few levels remain above the ionization limit up to $Z=80$.

TABLE III. Total rate coefficients S^{EA} for excitation-autoionization through $3d^{10}4s^24p$-$3d^94s^24p4d,4f$ inner-shell excitations, in the Ga isoelectronic sequence. The rates have been calculated in the electron temperature range from 0.3 to 2 times the first ionization energy E_I. $X[-Y]$ means $X\times10^{-Y}$. The coefficients are given in $cm^3\,s^{-1}$ units.

Element	Z \ T_e	$0.3E_I$	$0.5E_I$	$0.7E_I$	$1.0E_I$	$2.0E_I$
Zr	40	9.60[−11]	4.36[−10]	8.10[−10]	1.24[−9]	1.88[−9]
Nb	41	8.28[−11]	3.83[−10]	7.05[−10]	1.08[−9]	1.64[−9]
Mo	42	8.01[−11]	3.65[−10]	6.62[−10]	1.01[−9]	1.51[−9]
Tc	43	8.04[−11]	3.47[−10]	6.29[−10]	9.46[−10]	1.40[−9]
Ru	44	8.15[−11]	3.43[−10]	6.13[−10]	9.07[−10]	1.33[−9]
Rh	45	7.89[−11]	3.26[−10]	5.69[−10]	8.40[−10]	1.22[−9]
Pd	46	7.60[−11]	3.08[−10]	5.37[−10]	7.87[−10]	1.14[−9]
Ag	47	7.23[−11]	2.83[−10]	4.91[−10]	7.17[−10]	1.03[−9]
Cd	48	6.98[−11]	2.71[−10]	4.62[−10]	6.71[−10]	9.64[−10]
In	49	6.67[−11]	2.51[−10]	4.25[−10]	6.12[−10]	8.71[−10]
Sn	50	6.49[−11]	2.41[−10]	4.06[−10]	5.80[−10]	8.21[−10]
Sb	51	6.24[−11]	2.27[−10]	3.80[−10]	5.42[−10]	7.62[−10]
Te	52	5.75[−11]	2.09[−10]	3.47[−10]	4.94[−10]	6.96[−10]
I	53	5.41[−11]	1.94[−10]	3.21[−10]	4.55[−10]	6.39[−10]
Xe	54	5.13[−11]	1.82[−10]	3.00[−10]	4.24[−10]	5.93[−10]
Cs	55	4.88[−11]	1.73[−10]	2.80[−10]	3.93[−10]	5.41[−10]
Ba	56	4.73[−11]	1.62[−10]	2.64[−10]	3.69[−10]	5.06[−10]
La	57	4.48[−11]	1.49[−10]	2.41[−10]	3.36[−10]	4.66[−10]
Ce	58	4.12[−11]	1.39[−10]	2.24[−10]	3.12[−10]	4.30[−10]
Pr	59	2.37[−11]	8.49[−11]	1.37[−10]	1.96[−10]	2.81[−10]
Nd	60	2.22[−11]	7.82[−11]	1.26[−10]	1.78[−10]	2.54[−10]
Pm	61	2.09[−11]	7.06[−11]	1.18[−10]	1.63[−10]	2.32[−10]
Sm	62	1.78[−11]	5.94[−11]	9.66[−11]	1.36[−10]	1.92[−10]
Eu	63	1.24[−11]	4.02[−11]	6.43[−11]	8.90[−11]	1.23[−10]
Gd	64	1.05[−11]	3.45[−11]	5.52[−11]	7.65[−11]	1.06[−10]
Tb	65	8.65[−12]	2.88[−11]	4.63[−11]	6.51[−11]	9.28[−11]
Dy	66	6.42[−12]	2.14[−11]	3.44[−11]	4.81[−11]	6.95[−11]
Ho	67	5.82[−12]	1.90[−11]	3.06[−11]	4.29[−11]	6.06[−11]
Er	68	4.82[−12]	1.60[−11]	2.58[−11]	3.67[−11]	5.28[−11]
Tm	69	4.33[−12]	1.42[−11]	2.30[−11]	3.25[−11]	4.67[−11]
Yb	70	3.52[−13]	1.16[−12]	1.88[−12]	2.65[−12]	3.80[−12]
Lu	71	1.92[−13]	6.31[−13]	1.02[−12]	1.43[−12]	2.05[−12]
Hf	72	1.21[−13]	3.99[−13]	6.42[−13]	9.06[−13]	1.30[−12]
Ta	73	3.72[−14]	1.23[−13]	1.97[−13]	2.75[−13]	3.89[−13]
W	74	2.96[−14]	9.71[−14]	1.57[−13]	2.20[−13]	3.14[−13]
Re	75	2.48[−14]	8.19[−14]	1.31[−13]	1.84[−13]	2.63[−13]
Os	76	1.94[−14]	6.33[−14]	1.02[−13]	1.43[−13]	2.05[−13]
Ir	77	2.51[−15]	7.71[−15]	1.18[−14]	1.57[−14]	2.02[−14]
Pt	78	1.98[−15]	6.05[−15]	9.20[−15]	1.22[−14]	1.53[−14]
Au	79	2.37[−16]	6.62[−16]	9.25[−16]	1.08[−15]	1.01[−15]
Hg	80	1.30[−16]	3.58[−16]	4.94[−16]	5.70[−16]	5.04[−16]
Tl	81	0	0	0	0	0

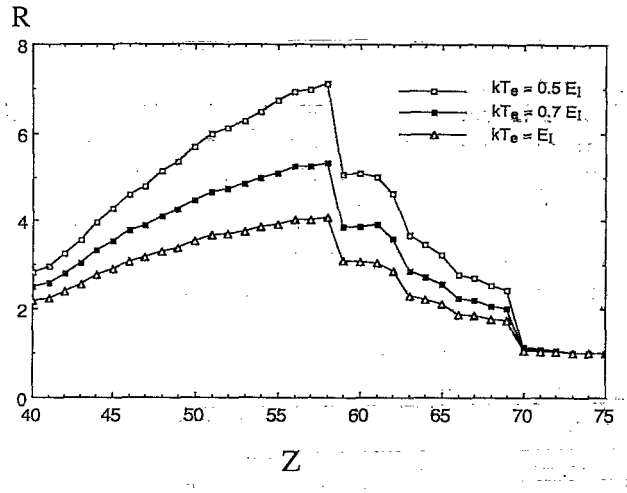

FIG. 5. Ratio R of total ionization rate coefficient ($S^{EA}+S$) to direct ionization rate coefficient S, at electron temperatures equal to 0.5, 0.7, and 1.0 times the first ionization energy E_I for each ion, as a function of Z, in the Ga isoelectronic sequence.

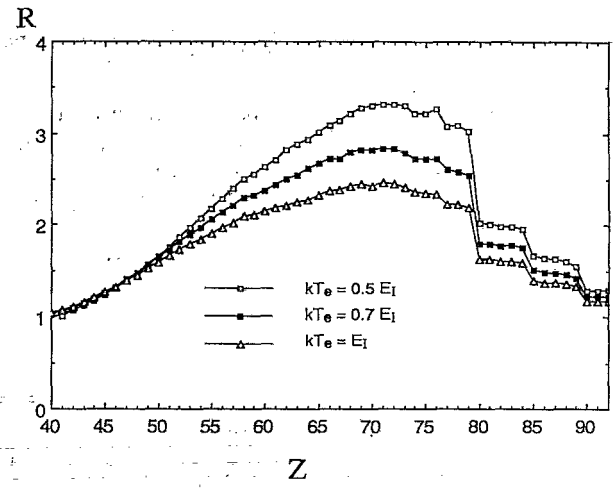

FIG. 6. Ratio R of total ionization rate coefficient ($S^{EA}+S$) to direct ionization rate coefficient S, at electron temperatures equal to 0.5, 0.7, and 1.0 times the first ionization energy E_I for each ion, as a function of Z, in the Kr isoelectronic sequence.

E. Kr isoelectronic sequence

The processes calculated in this sequence involve collisional excitation from the ground state $3d^{10}4s^24p^6$ to the inner-shell excited configurations $3d^94s^24p^64l$ ($l=d,f$), radiative decay from these configurations to the ground state and to $3d^{10}4s^24p^54d$ and $3d^{10}4s^24p^54f$, and autoionization from the inner-shell excited configurations to the configurations $3d^{10}4s^24p^5$, $3d^{10}4s4p^6$, $3d^{10}4s^24p^44d$, and $3d^{10}4s^24p^44f$ of the Br-like ions. Because of the complexity of the computations, no attempt was made to include in this sequence the configuration mixing effects. Besides, these effects are expected to have a small impact on the total EA rates, since the inner-shell excited configurations lie well above the ionization limit. $4f\rightarrow 4d$ radiative decays between the inner-shell excited levels are not taken into account here since most of the $3d^94s^24p^64d$ levels lie above the ionization limit, and thus these radiative decays would be followed primarily by further autoionization. Table IV displays the results for the total rate coefficients S^{EA} through $3d$-$4l$ inner-shell excitations for the elements with $40\leq Z\leq 92$. Figure 6 shows the ionization enhancement ratio R at the three different electron temperatures. The smooth increase of R for $Z<70$ is due to the progressive lowering, along the isoelectronic sequence, of the inner-shell excited autoionizing levels lying well above the ionization limit at low Z; this gradually favors the excitation processes with respect to direct ionization. Other processes which have an effect opposite to the above trend are the closing of autoionizing channels and the relative increase of radiative transitions to lower levels (nonautoionizing); these start to become important only for high-Z elements. Thus the general decreasing trend, observed in the previous isoelectronic sequences, appears here only for $Z\geq 70$; a first significant drop occurs at $Z=80$, followed by a few further gradual steps until $Z=92$. In this sequence, the factor R peaks for $kT_e=0.7E_I$ at only 2.8. Indeed, for these ions the $3d$ electrons are screened by eight $4l$ outer electrons causing the electron-impact excitation of the $3d$ electrons to be less effective at relevant electron temperatures.

One should notice that the configurations $3d^{10}4s4p^64l$ lie below the first ionization limit for all the elements with $Z\geq 41$. In lower-Z range, these configurations are autoionizing and the contribution to EA has been computed and found to be even larger than that of $3d^94s^24p^64l$. However, the absolute contribution of the $4s$ inner-shell excited configurations is only about a few percent of the total direct ionization rate, and thus it is also not included for $Z=40$ in the present work.

F. Other isoelectronic sequences

In the intermediate Ge to Br isoelectronic sequences (ground state $3d^{10}4s^24p^m$, $m=2$ to 5), detailed computations have been performed at the beginning for Mo ($Z=42$), Xe ($Z=54$), Pr ($Z=59$), and Dy ($Z=66$) only. For these isoelectronic sequences, due to the complexity of the configurations which contain hundreds of levels, the detailed calculations are quite tedious. In the present work, the following main configurations have been taken into account: for the initial ion, the ground state, the main inner-shell excited configurations $3d^94s^24p^m4l$ ($l=p,d,f$), and the low-lying configurations $3d^{10}4s^24p^{m-1}4l$ ($l=d,f$), and for the next ionization state, the ground state and the configurations $3d^{10}4s^24p^{m-2}4l$ ($l=d,f$) and $3d^{10}4s4p^m$ (the ones that can be produced by autoionization from the main inner-shell configurations $3d^94s^24p^m4l$).

In these sequences, the detailed EA computations have been carried out for the four elements mentioned with two objectives. First, we used the results in the fractional

TABLE IV. Total rate coefficients S^{EA} for excitation-autoionization through $3d^{10}4s^24p^6$-$3d^94s^24p^64d,4f$ inner-shell excitations, in the Kr isoelectronic sequence. The rates have been calculated in the electron temperature range from 0.3 to 2 times the first ionization energy E_I, $X[-Y]$ means $X\times10^{-Y}$. The coefficients are given in $cm^3\,s^{-1}$ units.

Element	T_e / Z	$0.3E_I$	$0.5E_I$	$0.7E_I$	$1.0E_I$	$2.0E_I$
Zr	40	1.62[−12]	3.25[−11]	1.12[−10]	2.69[−10]	6.62[−10]
Nb	41	3.47[−12]	5.09[−11]	1.53[−10]	3.32[−10]	7.40[−10]
Mo	42	5.98[−12]	7.00[−11]	1.91[−10]	3.87[−10]	7.97[−10]
Tc	43	8.82[−12]	8.66[−11]	2.20[−10]	4.22[−10]	8.16[−10]
Ru	44	1.17[−11]	1.00[−10]	2.40[−10]	4.45[−10]	8.19[−10]
Rh	45	1.47[−11]	1.12[−10]	2.58[−10]	4.57[−10]	8.17[−10]
Pd	46	1.74[−11]	1.22[−10]	2.65[−10]	4.61[−10]	8.00[−10]
Ag	47	1.99[−11]	1.28[−10]	2.75[−10]	4.63[−10]	7.86[−10]
Cd	48	2.19[−11]	1.33[−10]	2.72[−10]	4.51[−10]	7.47[−10]
In	49	2.35[−11]	1.35[−10]	2.72[−10]	4.42[−10]	7.17[−10]
Sn	50	2.53[−11]	1.36[−10]	2.69[−10]	4.30[−10]	6.91[−10]
Sb	51	2.65[−11]	1.35[−10]	2.63[−10]	4.18[−10]	6.58[−10]
Te	52	2.70[−11]	1.35[−10]	2.57[−10]	4.03[−10]	6.25[−10]
I	53	2.80[−11]	1.33[−10]	2.48[−10]	3.84[−10]	5.89[−10]
Xe	54	2.79[−11]	1.29[−10]	2.39[−10]	3.66[−10]	5.54[−10]
Cs	55	2.84[−11]	1.26[−10]	2.30[−10]	3.49[−10]	5.24[−10]
Ba	56	2.88[−11]	1.23[−10]	2.22[−10]	3.32[−10]	4.93[−10]
La	57	2.84[−11]	1.20[−10]	2.12[−10]	3.15[−10]	4.64[−10]
Ce	58	2.80[−11]	1.16[−10]	2.06[−10]	3.03[−10]	4.35[−10]
Pr	59	2.72[−11]	1.08[−10]	1.88[−10]	2.79[−10]	4.05[−10]
Nd	60	2.64[−11]	1.03[−10]	1.78[−10]	2.60[−10]	3.78[−10]
Pm	61	2.55[−11]	9.85[−11]	1.69[−10]	2.45[−10]	3.55[−10]
Sm	62	2.42[−11]	9.55[−11]	1.60[−10]	2.31[−10]	3.29[−10]
Eu	63	2.39[−11]	9.08[−11]	1.51[−10]	2.16[−10]	3.07[−10]
Gd	64	2.32[−11]	8.51[−11]	1.46[−10]	2.04[−10]	2.89[−10]
Tb	65	2.27[−11]	8.17[−11]	1.39[−10]	1.94[−10]	2.72[−10]
Dy	66	2.16[−11]	7.80[−11]	1.32[−10]	1.87[−10]	2.56[−10]
Ho	67	2.07[−11]	7.38[−11]	1.22[−10]	1.75[−10]	2.39[−10]
Er	68	2.03[−11]	7.09[−11]	1.18[−10]	1.67[−10]	2.26[−10]
Tm	69	1.97[−11]	6.75[−11]	1.11[−10]	1.57[−10]	2.12[−10]
Yb	70	1.87[−11]	6.35[−11]	1.03[−10]	1.44[−10]	1.98[−10]
Lu	71	1.76[−11]	5.96[−11]	9.65[−11]	1.37[−10]	1.85[−10]
Hf	72	1.65[−11]	5.54[−11]	9.00[−11]	1.27[−10]	1.72[−10]
Ta	73	1.54[−11]	5.13[−11]	8.20[−11]	1.16[−10]	1.56[−10]
W	74	1.39[−11]	4.63[−11]	7.41[−11]	1.04[−10]	1.41[−10]
Re	75	1.32[−11]	4.34[−11]	6.94[−11]	9.71[−11]	1.31[−10]
Os	76	1.25[−11]	4.15[−11]	6.49[−11]	8.97[−11]	1.22[−10]
Ir	77	1.11[−11]	3.56[−11]	5.67[−11]	7.72[−11]	1.04[−10]
Pt	78	1.05[−11]	3.38[−11]	5.26[−11]	7.25[−11]	9.63[−11]
Au	79	9.79[−12]	3.10[−11]	4.85[−11]	6.65[−11]	8.90[−11]
Hg	80	4.30[−12]	1.47[−11]	2.36[−11]	3.34[−11]	4.78[−11]
Tl	81	4.08[−12]	1.36[−11]	2.21[−11]	3.11[−11]	4.45[−11]
Pb	82	3.81[−12]	1.26[−11]	2.04[−11]	2.86[−11]	4.08[−11]
Bi	83	3.64[−12]	1.19[−11]	1.93[−11]	2.70[−11]	3.83[−11]
Po	84	3.36[−12]	1.10[−11]	1.77[−11]	2.47[−11]	3.52[−11]
At	85	2.26[−12]	7.20[−12]	1.14[−11]	1.58[−11]	2.20[−11]
Rn	86	2.06[−12]	6.51[−12]	1.03[−11]	1.43[−11]	2.00[−11]
Fr	87	1.94[−12]	6.11[−12]	9.67[−12]	1.34[−11]	1.87[−11]
Ra	88	1.77[−12]	5.56[−12]	8.81[−12]	1.22[−11]	1.71[−11]
Ac	89	1.54[−12]	4.86[−12]	7.73[−12]	1.07[−11]	1.52[−11]
Th	90	7.41[−13]	2.38[−12]	3.80[−12]	5.30[−12]	7.52[−12]
Pa	91	6.97[−13]	2.22[−12]	3.54[−12]	4.93[−12]	6.99[−12]
U	92	6.93[−13]	2.19[−12]	3.48[−12]	4.82[−12]	6.80[−12]

abundance coronal calculations performed for these elements (Sec. VI). Additionally, these EA computations for a few elements constitute a check of the accuracy of the approximate treatment developed for the other elements in the Ge to Br sequences; thus the EA results for these sequences will be presented in terms of the mean branching ratio, as explained in the next section.

In the Ni-like ions, there are no $3d$-$4l$ EA processes, since the ground-state configuration of these ions is $3d^{10}$. On the other hand, although the rates for the $3p$-$4l$ inner-shell excitations are not negligible compared to the total direct ionization rates, very few levels of the $3p^5 3d^{10} 4l$ configurations are autoionizing even for $Z=40$. For $Z \geq 42$ all the levels lie totally below the ionization limit. Therefore $3p$-$4l$ EA processes were not considered in the coronal balance calculations.

The EA effect will also not be considered in the adjacent preceding sequences (Co, Fe, etc.)

On the other side of the Kr sequence, in Rb-, Sr-, and Y-like ions, the $3d$-$4d$ and $3d$-$4f$ EA rate coefficients will be estimated by extrapolation of Kr results; this approximation leads to an acceptable range of error, since the contribution of these EA processes to the total ionization rate is expected to be relatively less important here. Indeed, the $3d$ inner-shell excited levels lie very high above the ionization limit, and furthermore, there are many electrons in the $n=4$ outer shells which contribute to direct ionization.

V. AVERAGE METHOD FOR EA RATE EVALUATION

A. Mean autoionization branching ratio $\bar{B}$

The drastic change in the EA rates along an isoelectronic sequence can be analyzed well through the use of a mean branching ratio method, as proposed by Cowan and Mann [8]. Moreover, it permits, in a rather simple way, the introduction of the EA processes in the ionization balance equations. Also, it gives a way to evaluate the EA rates through $3d$-$4l$ inner-shell excitations in many of the cases or sequences where detailed computations are not performed due to the very large number of levels involved.

The mean branching ratio for autoionization for the whole inner-shell excited configuration J is defined by

$$\overline{B_J} = \sum_{j \in J} \left[\frac{Q_{gj} \sum_k A^a_{jk}}{\sum_i A_{ji} + \sum_k A^a_{jk}} \right] \Big/ \sum_{j \in J} Q_{gj} \equiv \sum_{j \in J} Q_{gj} B^a_j \Big/ \sum_{j \in J} Q_{gj} , \quad (4)$$

thus

$$S^{\mathrm{EA}}_J = \overline{B_J} \sum_{j \in J} Q_{gj} . \quad (5)$$

In Eqs. (4) and (5) above, all the quantities refer to those defined in Eq. (1). The summation is performed over all levels j belonging to the configuration J, and S^{EA}_J represents the contribution of the intermediate inner-shell excited configuration J to the total S^{EA} rate coefficient.

B. Calculation of $\bar{B}$ using detailed computations

Using the detailed computations of Sec. IV, the mean autoionization branching ratios are calculated separately for the $3d^9 4s^m 4p^n 4d$ and $3d^9 4s^m 4p^n 4f$ inner-shell excited configurations in the Cu, Zn, Ga, and Kr isoelectronic sequences at different temperatures. Figures 7–10 present the results at a temperature corresponding to the first ionization energy of the ion considered. An important property of the mean branching ratio, which is found in the present analysis and observed also for the Na isoelectronic sequence [8], is that it is almost constant as a function of T_e in the range from 0.3 to 2 times the ionization energy E_I (with an accuracy generally better than 10%). Since the ion abundance is practically negligible outside this range, one can use a constant mean branching ratio approximation in the coronal ionization balance model.

Besides the effect due to the progressive closing of the autoionization channels, the behavior of the mean branching ratio along an isoelectronic sequence is dictated by the relative importance of the radiative decay rate coefficient A compared to the autoionization rate coefficient A^a. The mean branching ratio along an isoelectronic sequence is approximately equal to unity in neutral and weakly ionized atoms, but can be significantly less than unity for highly ionized atoms. Indeed, the Einstein coefficients A are not greater than $10^9\ \mathrm{s}^{-1}$ in neutral and weakly ionized species. These coefficients grow approximately as $(r+1)^4$ along the isoelectronic sequence for $\Delta n=1$ transitions, r being the ion charge number. On the other hand, the autoionization coefficients A^a are nearly independent of r; these are of the order of 10^{12}–$10^{14}\ \mathrm{s}^{-1}$. Thus a smooth decrease of $\bar{B}$ as a function of Z is expected. The results presented in Figs. 7–10 reflect quite well the predictions of the trend as Z increases along the isoelectronic sequences, shown by Figs.

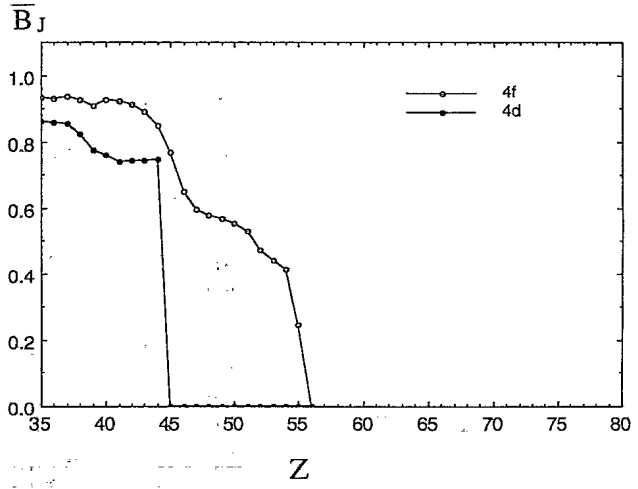

FIG. 7. Mean branching ratio for autoionization for $3d^9 4s 4d$ and $3d^9 4s 4f$ inner-shell excited intermediate configurations, at electron temperatures equal to the first ionization energy E_I for each ion, as a function of Z, in the Cu isoelectronic sequence.

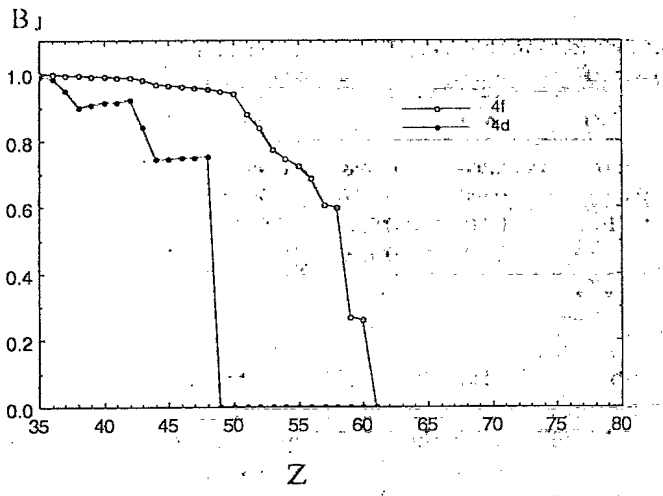

FIG. 8. Mean branching ratio for autoionization for $3d^9 4s^2 4d$ and $3d^9 4s^2 4f$ inner-shell excited intermediate configurations, at electron temperatures equal to the first ionization energy E_I for each ion, as a function of Z, in the Zn isoelectronic sequence.

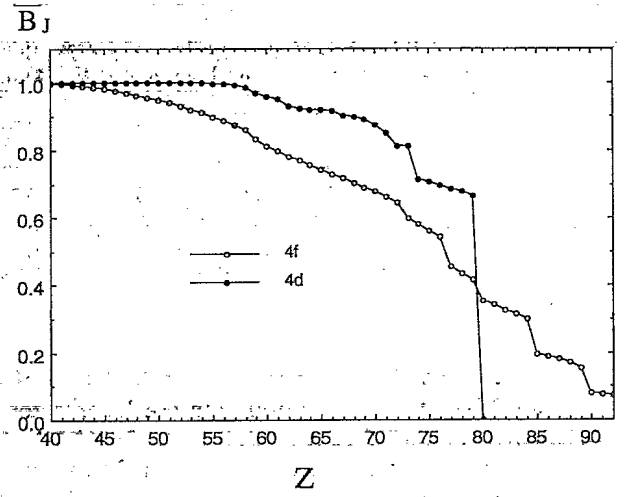

FIG. 10. Mean branching ratio for autoionization for $3d^9 4s^2 4p^6 4d$ and $3d^9 4s^2 4p^6 4f$ inner-shell excited intermediate configurations, at electron temperatures equal to the first ionization energy E_I for each ion, as a function of Z, in the Kr isoelectronic sequence.

1 and 2. As the excited levels fall below the ionization limit, the mean branching ratio for autoionization falls. This occurs first for the $4d$ inner-shell excited configuration and then for the $4f$ configuration. This effect is far more important than the smooth lowering of the branching ratio due to the increase of the radiative decay with r.

For Mo, Xe, Pr, and Dy, detailed calculations are performed for all the isoelectronic sequences from Cu to Kr, and results of the mean autoionization branching ratios calculated at $kT_e = E_I$ are given in Table V (for $3d$-$4d$ inner-shell excitation) and in Table VI (for $3d$-$4f$ excitation).

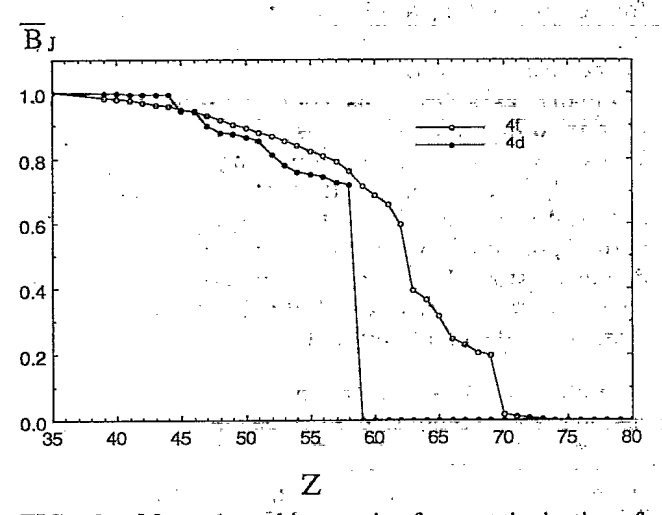

FIG. 9. Mean branching ratio for autoionization for $3d^9 4s^2 4p 4d$ and $3d^9 4s^2 4p 4f$ inner-shell excited intermediate configurations, at electron temperatures equal to the first ionization energy E_I for each ion, as a function of Z, in the Ga isoelectronic sequence.

C. Analytical expression for the total excitation rate coefficient

In order to estimate the EA rates using the constant mean branching ratio approximation, it is necessary to calculate the total collisional excitation rate coefficient $\sum_{j \in J} Q_{gj}$ for the whole configuration J appearing in expression (5), as a function of the electron temperature T_e.

It is found in the framework of the present work that the results of the distorted-wave calculations for the collisional excitation total rate coefficients as a function of T_e can be described using an approximate analytical formula. This formula is based on the often-used Van Regemorter semiempirical expression [22]. The total excitation rate coefficient through $3d$-$4d$ or $3d$-$4f$ electron-impact excitation can be written as follows:

$$Q_{gJ}(T_e) = \sum_{j \in J} Q_{gi} = 1.58 \times 10^{-5} \frac{\sqrt{\beta_J}}{e^{\beta_J} E_J^{3/2}} f_{gJ} G(r, \beta_J) , \tag{6}$$

where

$$\beta_J = \frac{E_J}{kT_e} \tag{7}$$

and

$$f_{gJ} G(r, \beta_J) = a(r) + \frac{b(r)}{\beta_J} + c(r) \ln \beta_J . \tag{8}$$

Q_{gJ} is in units of $\mathrm{cm^3\,s^{-1}}$. E_J is the average energy of the $3d^9 4s^m 4p^n 4d$ or $3d^9 4s^m 4p^n 4f$ inner-shell excited configuration (in eV). f_{gJ} is the average oscillator strength and $G(r, \beta_J)$ is an effective Gaunt factor; r is the ion charge number. Best fitting expressions for the parameters a, b, and c as a function of r are given in Table VII.

TABLE V. Mean branching ratio $\overline{B_{4d}}$ for autoionization for $3d^9 4s^m 4p^n 4d$ inner-shell excited configurations, at electron temperatures equal to the first ionization energy E_I of each ions, for Cu- to Kr-like Mo, Xe, Pr, and Dy ions. 0.4[−4] means 0.4×10^{-4}.

Element	Z	Cu I	Zn I	Ga I	Ge I	As I	Se I	Br I	Kr I
Mo	42	0.741	0.919	0.995	0.997	0.994	0.998	0.999	0.999
Xe	54	0	0	0.755	0.897	0.940	0.977	0.993	0.997
Pr	59	0	0	0	0.716	0.803	0.938	0.952	0.969
Dy	66	0	0	0	0.4[−4]	0.591	0.758	0.900	0.914

The expressions above permit a fast calculation of the $3d$-$4d$ and $3d$-$4f$ total excitation rate coefficients for all the elements (in the Z range relevant to $3d$-$4l$ EA processes) in the isoelectronic sequences from Cu to Kr, and for $0.2E_I \le kT_e \le 2.0E_I$. The results reproduce the distorted-wave detailed computation results with an accuracy between 1% and 5%, except for low-charge ions ($r<10$).

D. Analytical expression for the average inner-shell transition energies

The average excitation energy E_J for the $3d$-$4d$ or $3d$-$4f$ transitions, necessary for the calculation of Q_{gJ} through the approximate expression (6), can be obtained directly using the following analytical expression:

$$E_J=\sigma_{\rm H}^J(r+1)^2+A+B(r+1)+C(r+1)^2 . \quad (9)$$

E_J is given in eV, $\sigma_{\rm H}^J=R_\infty(1/3^2-1/4^2)=0.661\,39$ eV is the hydrogenic term, and r is the ion charge number. A,B,C are constant parameters (in eV) given in Table VIII, calculated by a best fit method for each isoelectronic sequence and for both $3d$-$4d$ and $3d$-$4f$ inner-shell excitations. This formula reproduces the average transition energies with an accuracy better than 0.5% compared to the detailed computations using the RELAC method for all the sequences considered and for the elements with $40\le Z\le 92$.

E. Direct procedure for a fast $S^{\rm EA}$ evaluation

Using the total excitation rate coefficients given in analytic form [expression (6)] together with the mean branching ratios shown in Figs. 7–10, one can reproduce the results of the EA rate coefficients of Sec. IV directly in the sequences Cu, Zn, Ga, and Kr, following Eq. (5). This procedure permits one to estimate the partial contribution $S_J^{\rm EA}$ for each of the two main inner-shell excitations, and also allows one to obtain a continuous T_e dependence through the total excitation rate coefficients.

Moreover, for the other sequences from Ge to Br, one can get easily acceptable interpolated values of the mean branching ratio for all the elements (besides Mo, Xe, Pr, and Dy) for which detailed computations were not performed. This can be done by a linear interpolation (as a function of r) between the calculated $\overline{B_J}$ values for the Ga- and Kr-like ions for a given element. However, this procedure is valid only in the Z range where no significant $\overline{B_J}$ discontinuities are expected for the Ge to Br sequences. Figures 11 and 12 show that the interpolation is possible in the range $Z\le 58$ for $3d$-$4d$ excitation and $Z\le 69$ for $3d$-$4f$.

A better alternative procedure which applies for the whole $40\le Z\le 92$ range consists of interpolating (or extrapolating) the data obtained for the four elements Mo, Xe, Pr, and Dy along each one of the Ge to Br sequences; the data for these elements have been plotted in Figs. 11 and 12. However, the results for these four elements are not sufficient for an accurate interpolation (or extrapolation) due to the expected discontinuities. For this purpose we have performed new detailed computations to determine $\overline{B_J}$ for other ions around each zone where along the Ge to Br sequences an abrupt drop in the $\overline{B_J}$ curves is expected. These new results are also shown in Figs. 11 and 12, in addition to the previous results for the four elements Mo, Xe, Pr, and Dy. These data now permit a more accurate interpolation along the whole sequence from Ge to Br.

Finally, as a test, this approximation procedure has been tried in a few specific cases for these four sequences. Using the estimated mean branching ratios together with the analytical excitation rate coefficient formula (6), final $S^{\rm EA}$ values are obtained at a temperature equal to E_I, with a precision compared to those calculated using the detailed distorted-wave method of better than 5%. In the general case, an accuracy of about 10% for the approximate method can be expected.

TABLE VI. Mean branching ratio $\overline{B_{4f}}$ for autoionization for $3d^9 4s^m 4p^n 4f$ inner-shell excited configurations, at electron temperatures equal to the first ionization energy E_I of each ion, for Cu- to Kr-like Mo, Xe, Pr, and Dy ions.

Element	Z	Cu I	Zn I	Ga I	Ge I	As I	Se I	Br I	Kr I
Mo	42	0.911	0.987	0.970	0.976	0.987	0.989	0.976	0.992
Xe	54	0.415	0.742	0.836	0.848	0.857	0.868	0.898	0.910
Pr	59	0	0.269	0.715	0.777	0.794	0.800	0.818	0.830
Dy	66	0	0	0.245	0.423	0.656	0.698	0.745	0.728

TABLE VII. Analytical expressions for the parameters $a(r)$, $b(r)$, and $c(r)$ appearing in the calculation of 3d-4d and 3d-4f inner-shell excitation rate coefficients of the ions belonging to the Kr to Cu isoelectronic sequences.

Transition	Parameter	Analytical expression
3d-4d	a	$0.745-462\times10^{-3}\exp(-73.5\times10^{-3}r)$
3d-4d	b	$-0.0936+1.25\times10^{-3}r$
3d-4d	c	$-0.109+1.32\times10^{-3}r$
3d-4f	a	$-0.211+81.4\times10^{3}r-0.779\times10^{-3}r^2$
3d-4f	b	$0.0157+12.6\times10^{-3}r-0.135\times10^{-3}r^2$
3d-4f	c	$0.0697-11.1\times10^{-3}r+0.139\times10^{-3}r^2$

VI. CORONAL IONIZATION RATE EQUATIONS

A. Calculation

The results of the preceding EA rate calculations are introduced in the ionization rate equations to calculate the EA effect on the plasma ionization balance. In this work, the ionization balance at steady state is calculated using the coronal model [23,24] which applies to optically thin, hot plasmas at low densities, like tokamak plasmas [20]. In this model, excitation of ions is due to electron impact, and all excited ions undergo radiative decay rather than collisional decay to lower excited levels. Finally, they return by cascading to the ground state in times that are short compared with the electron-ion inelastic collision time. Thus ionization (direct and EA) is essentially from the ground state, and is balanced in this regime by direct radiative and dielectronic recombinations. Electron velocity distribution is assumed to be Maxwellian. The relative abundance of two consecutive ions, in a coronal plasma at steady state, is given by

$$\frac{n_{r+1}}{n_r}=\frac{S_r+S_r^{\mathrm{EA}}}{\alpha_{r+1}}, \qquad (10)$$

where n_{r+1} and n_r are the number densities of ions of charge $r+1$ and r, respectively. S_r is the rate coefficient for direct collisional ionization, and S_r^{EA} is the rate coefficient for excitation-autoionization from the ground state of ion r. α_{r+1} is the total recombination rate coefficient from ionization stage $r+1$ to stage r, and is equal to the sum $\alpha_{r+1}^{R}+\alpha_{r+1}^{D}$ of the rate coefficients for radiative and dielectronic recombinations, respectively. The fractional abundances $f_r=n_r/\sum_r n_r$ for a given element as a function of T_e are obtained by solving the set of equations (10) relative to all ionization stages and setting $\sum_r f_r=1$.

The direct ionization rate coefficients S_r are calculated here using the Lotz formula [Eq. (3)]. The S^{EA} coefficients are introduced using the simplified mean branching ratio method deduced from the results of the detailed calculations, as described in the preceding section.

Differential theoretical methods for calculating the radiative recombination cross sections and rate coefficients have been proposed (see, for instance, Ref. [25]). In the present work, the approximate expression proposed by Von Goeler *et al.* [26] for ionized atoms, based on the hydrogenic formula [27] is used in order to enable simple calculations. Moreover, this approximation was used already for coronal ion abundance predictions in tokamak plasmas [20], and thus, the use of the same formula permits a direct comparison between previous results and our calculations which take into account the EA processes. This expression is given in Appendix B.

Extensive theoretical studies of dielectronic recombination processes have been carried out (see, for instance, Refs. [28, and 29]). There are no data available for the complex ions considered here. In the present calculations the dielectronic recombination is introduced, for simplicity, through the Burgess-Merts approximate formula [30,31]. It has been noticed that the Burgess-Merts formula can overestimate the dielectronic recombination [32]. To account for this overestimation only two reso-

TABLE VIII. Parameters of the analytical approximate expression for the average energy of the inner-shell excited configurations $3d^9 4s^m 4p^n 4d$ and $3d^9 4s^m 4p^n 4f$.

	$3d^9 4s^m 4p^n 4d$			$3d^9 4s^m 4p^n 4f$		
Sequence	A	B	C	A	B	C
Cu I	−4.3426	11.475	5.814[−3]	−5.0628	14.796	1.626[−2]
Zn I	1.8317	12.699	2.923[−3]	1.2386	16.271	1.191[−2]
Ga I	13.3316	13.636	3.930[−3]	18.866	17.118	1.594[−2]
Ge I	24.900	14.594	4.841[−3]	30.919	18.343	1.525[−2]
As I	37.356	15.618	4.593[−3]	50.830	19.115	2.130[−2]
Se I	47.965	16.820	1.485[−3]	56.699	21.043	9.040[−3]
Br I	61.112	17.900	2.642[−4]	70.114	22.394	6.001[−3]
Kr I	75.353	18.963	−3.074[−4]	82.799	23.914	9.583[−4]

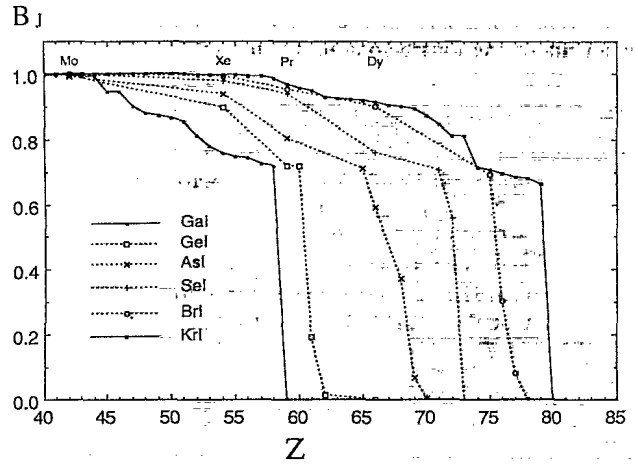

FIG. 11. Mean branching ratio for autoionization for $3d^9 4s^2 4p^m 4d$ ($m=2$ to 5) inner-shell excited intermediate configurations, at electron temperatures equal to the first ionization energy E_I, for a few elements along the Ge I to Br I sequences. In this figure, the Ga I and Kr I full curves have also been reported.

nant transitions are included in the calculations, as suggested by Breton, De Michelis, and Mattioli [20]. This formula is chosen also for the purpose of comparing our results to previous tokamak calculations using this approximation. The calculation method based on the Burgess-Merts formula is described in Appendix C.

Although the methods of evaluating the recombination contribution are quite approximate, it must be emphasized that the principal aim of the present work is to analyze the *relative* effect of EA on the ionization balance. Thus, even if the absolute values for the temperatures of maximum ion abundances, as obtained in the present model, have some inaccuracy due to the rough estimation of the recombination processes, the relative shift of these temperatures due to the EA processes should be reliable.

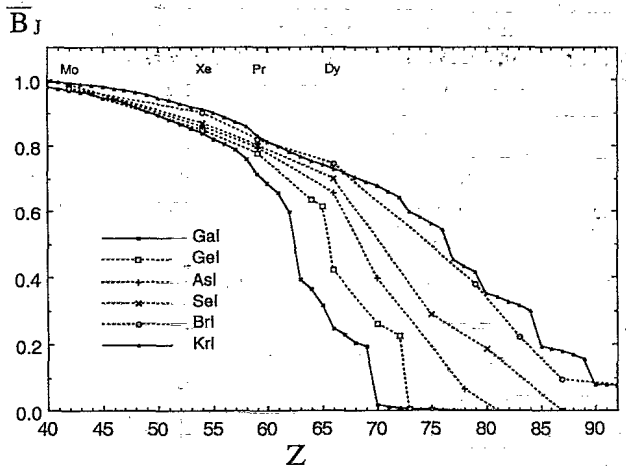

FIG. 12. Mean branching ratio for autoionization for $3d^9 4s^2 4p^m 4f$ ($m=2$ to 5) inner-shell excited intermediate configurations, at electron temperatures equal to the first ionization energy E_I, for a few elements along the Ge I to Br I sequences. In this figure, the Ga I and Kr I full curves have also been reported.

B. Results

In order to investigate the EA effect on the fractional ion abundances, the system of steady state equations (10) has been solved for the four elements Mo, Xe, Pr, and Dy. Figure 13(a) shows the results of calculation of fractional ion abundances for Kr- to Co-like praseodymium ions (Pr^{+23}-Pr^{+32}) obtained by setting $S^{EA}=0$ [i.e., without taking into account the EA processes in Eqs. (10)], whereas Fig. 13(b) shows the results obtained by including the EA processes. In principle, the system of Eqs. (10) should include all the ionization stages of the element starting from the neutral atom. However, in practice a simplification can be made by considering a reduced number of ionization stages in the equation system, around the Kr to Cu sequences; for these sequences the main EA process, through $3d$-$4l$ inner-shell excitation, was found to be the most significant. For the Rb-like and adjacent lower-charged ions the EA processes become less and less important, whereas for the Ni-like and adjacent higher-charged ions the EA effect can be neglected (Sec. IV F). The fractional abundance for a given ionization stage, which is a function of T_e only in the steady state coronal model, is directly related to that of the next lower and higher stages; it is affected very little by any change in the abundance of distant ionization stages. Therefore it is not necessary here to calculate all the atomic quantities for all the other sequences; notably, the lower ionization stages of the heavy elements which involve very cumbersome computations can be ignored.

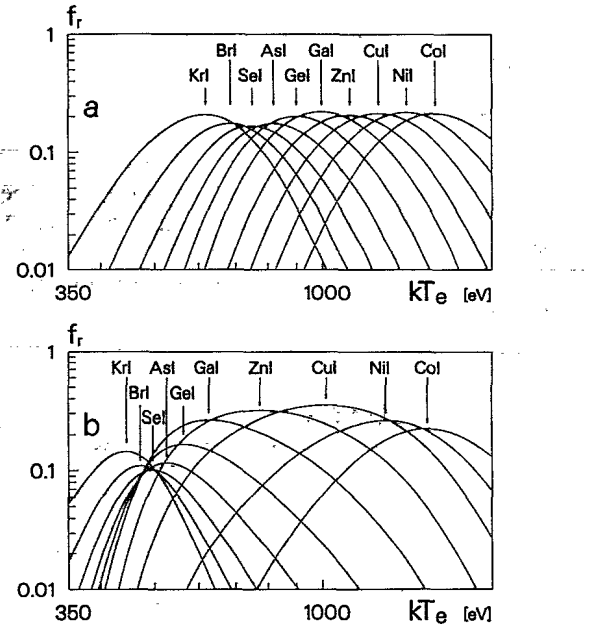

FIG. 13. Fractional abundances for Kr I- to Co I-like praseodymium ions (Pr^{+23}–Pr^{+32}) as functions of electron temperature: (a) without excitation-autoionization process, and (b) including excitation-autoionization processes. The maximum abundance for each ion is indicated by an arrow.

The addition of only a few adjacent ionization stages is needed. The number of additional ionization stages is determined by the accuracy desired. In the present work, after successive tries, three lower ionization stages preceding the Kr sequence (Y-, Sr-, and Rb-like ions) and five higher ionization stages following the Cu sequence (Ni- to Cr-like ions) have been included. For ions pertaining to the Y, Sr, and Rb sequences, approximate EA rate coefficients deduced from an extrapolation of the mean branching ratios of the Kr to Cu sequences, are used. For the Ni to Cr isoelectronic sequences EA processes have been neglected as indicated in Sec. IV F. Neglecting other sequences in the rate equations introduces an estimated error of less than 1% in the temperatures of maximum ion abundances for all the sequences studied.

The striking general trend observed in Fig. 13(b) is an important shift of the first curves towards lower temperatures, resulting from the enhancement of the total ionization rate due to EA processes. A similar effect is obtained also in the present work for the fractional abundances of the other elements: Mo, Xe, and Dy (not displayed here).

In the case of praseodymium ($Z=59$), the Cu-like ion has a relatively large fractional abundance, spread over a wide T_e domain, as shown in Fig. 13(b). This is due to the fact that the ionization of this ion is no longer increased by any EA process (see Fig. 3), whereas its creation is still favored by an EA contribution to the ionization of the Zn-like ion (although through $3d$-$4f$ only, as shown in Fig. 4). This behavior changes with Z. For dysprosium ($Z=66$), the results show that the same effect occurs; however, in this case, the Zn- and Ga-like ion fractional abundances are the largest, since for this element there is no EA contribution from the Zn-like ion (see Fig. 4).

The ionization rate coefficient enhancement factor R due to EA processes is a function of the electron temperature for each ion. In order to show the correct magnitude of the EA effect one has to calculate the enhancement factor in the relevant temperature range, i.e., around the electron temperature $T_{\max}$ of maximum abundance for each ion (in the coronal model). These temperatures are deduced from the solution of the system of Eqs. (10) for the successive ions around the sequences investigated in Mo, Xe, Pr, and Dy. Figure 14 displays the ionization enhancement factor $R(T_{\max})$ calculated at the temperature of maximum abundance for the various ions. These R values are slightly different and, in some cases, even much larger than the enhancement factors calculated *a priori* for temperatures equal to 0.5, 0.7, and 1 times the ionization energy (Sec. IV, Figs. 3–6). This is the case particularly for low-Z elements (like Mo) for which the maximum abundance occurs at a temperature lower than $0.5E_I$.

The results presented in Fig. 14 demonstrate the importance of EA processes in the sequences isoelectronic to the fourth row elements. The analysis of the results shows that the ionization enhancement factor can reach a maximum value varying from 4 (As-like) to 8 (Ga- or Zn-like) for elements with Z ranging from 65 to 50, and it

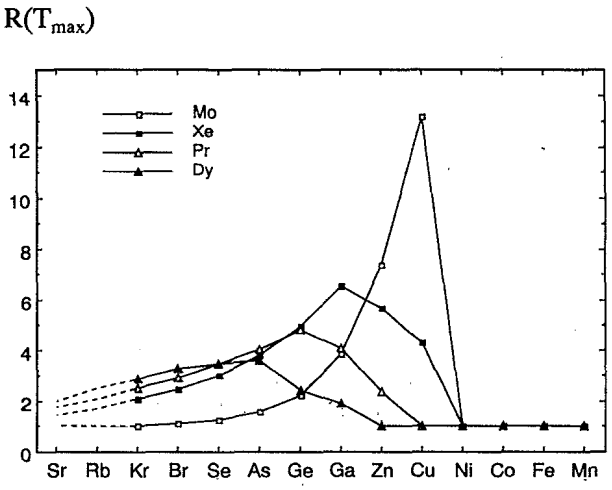

FIG. 14. Ratio R of total ionization rate coefficient ($S^{EA}+S$) to direct ionization rate coefficient S, at electron temperature $T_{\max}$ of maximum abundance in coronal plasma, for Kr- to Mn-like Mo, Xe, Pr, and Dy ions.

can be as high as 10 (Zn-like) to 14 (Cu-like) for lighter elements with Z from 47 to 40. The effects of EA processes on the ionization rates for these ions are much larger than for ions isoelectronic to the third row elements; for the Na sequence, a maximum enhancement between 2 and 3 was found [2,3,8].

The general trend of the EA effect of the ionization balance is summarized in Fig. 15. It shows the relative decrease of the electron temperature corresponding to the maximum ion abundance in coronal plasma, $\Delta T_{\max}/T_{0\,\max}$, due to EA processes [$T_{0\,\max}$ is the temperature of maximum ion abundance calculated using the

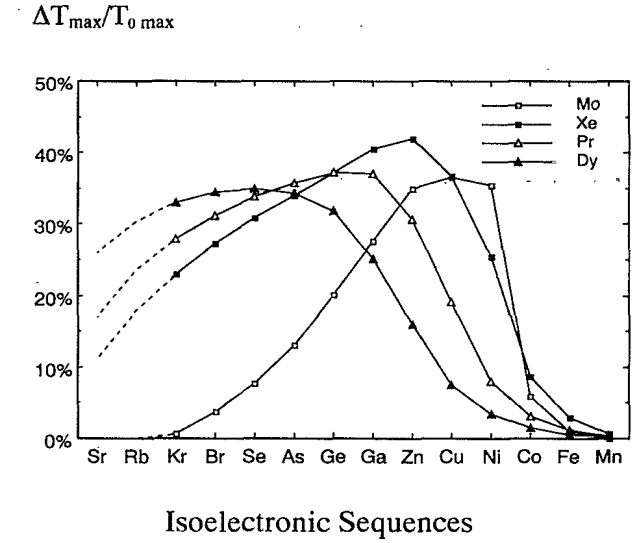

FIG. 15. Relative decrease of the electron temperature of maximum ion abundance due to EA processes in coronal plasma, for Kr- to Mn-like Mo, Xe, Pr, and Dy ions.

system of Eqs. (10) without the EA term]. The results are given for the successive ionization stages from Kr- to Mn-like ions in different Z regions: For Mo ($Z=42$), Xe ($Z=54$), Pr ($Z=59$), and Dy ($Z=66$). A very significant relative shift towards lower temperatures is observed for most of the ions; it can reach values up to 40%. The maximum shift occurs for different sequences as Z increases; it moves from Cu-like for molybdenum to Se-like for dysprosium. The small shift values in the Mo curve at low ionization sequences (Kr–Ge) in Fig. 15 reflect the small EA effect due to the very high relative position of the inner-shell excited configurations. On the other hand, the decrease in the Dy curve in the Ge–Cu sequences range reflects the closing of EA channels (as predicted in Figs. 11 and 12).

One notices a remarkable repercussion effect of the temperature shift of the fractional abundance from one ion to the adjacent one. This residual shift effect can be very important for Ni-like ions and is even noticeable for Co-like ions, although there are no more $3d$-$4l$ EA processes active in these sequences. Moreover, the smooth behavior of the $\Delta T_{\max}/T_{0\,\max}$ curves makes the prediction, by interpolation or extrapolation, of the temperature shift of maximum ion abundance, easy for other elements in the sequences from Kr to Mn.

VII. CONCLUSIONS

The present results have emphasized the significant and often dominant EA contribution to ionization processes in $3d^{10}4s^m4p^n$ ground configuration ions of the sequences isoelectronic to the fourth period elements. The lack of smooth behavior along the isoelectronic sequences has made extensive, level-by-level calculations necessary. These have been performed using the relativistic parameter potential code and the distorted-wave method. In the present work we have computed the EA contribution through the most important inner-shell excitations, those that occur via the $\Delta n=1$ $3d$-$4l$ transitions. The detailed computations have been done for all the elements from $Z=40$ to $Z=92$, along the Cu, Zn, Ga, and Kr isoelectronic sequences, at various electron temperatures, and have emphasized the importance of configuration mixing. The results have shown a general trend characterized by a smooth increase of the ionization rate enhancement due to EA as Z increases along the sequence, followed by a gradual decrease with some abrupt drops, reflecting the successive closings of autoionizing channels.

An average method has been developed to enable an approximate evaluation of the EA rates in other, more complex isoelectronic sequences (from Ge to Br), for all the elements with $40\leq Z\leq 92$. This average method is also intended to allow the introduction of the EA contribution into the ionization rate equations in an analytic form by means of tabulated parameters. The method is based on the use of a mean branching ratio for autoionization which is shown to be almost constant as a function of T_e.

The calculated ionization rate enhancement at $kT_e=E_I$ appears to be very significant for all the sequences within a large Z range. The EA effect is found to be even larger (mostly for light elements) in the relevant T_e range, i.e., around the temperature of maximum ion abundance in the coronal regime. The ionization enhancement $R(T_{\max})$ reaches a value of 6 around $Z=55$ (in the Ga sequence) and it is as high as 13 for $Z=42$ (Cu sequence).

The S^{EA} results presented in Tables I–IV constitute new basic data for the EA processes in the fourth row isoelectronic sequences. Although only the $3d$-$4l$ inner-shell excitations have been computed here, these represent the transitions which give the most important EA effect. Neglecting the EA processes via other inner-shell excitations like $3p$-$4l$, or $3p,d$-nl with $n\geq 5$ leads to an underestimation of the total EA rate. The largest EA contribution not considered here is via $3p$-$4l$, and is expected to be most important in the Cu sequence. Preliminary calculations indicate that neglecting this contribution may lead to an underestimation of the total (direct and EA) ionization rate of less than 10% in the $Z\leq 44$ elements, for which the $3d^9 4s4d$ configuration is still autoionizing. An error of more than 20% is expected for $45\leq Z\leq 54$. The contribution of the $3p$-$4l$ EA process is predicted to gradually decrease for the following sequences, and in addition the main $3d$-$4l$ EA effect extends to higher-Z domain (about $Z\leq 58$ for Zn I sequence, $Z\leq 69$ for Ga I, and $Z\leq 79$ for Kr I). More complex detailed calculations taking into account all these additional inner-shell excitations are planned.

Finally, the present S^{EA} data can be used for plasma ionization modeling. We have shown that the introduction of the main $3d$-$4l$ EA contribution to the coronal fractional ion abundance calculations leads to a very important shift towards lower temperatures in the electron temperature of maximum ion abundance; the relative temperature decrease can reach values up to 40%. The maximum shift occurs for a different sequence as Z increases; it moves from Cu-like for $Z=40$ to Se-like for $Z=66$.

The ionization and recombination rate coefficients introduced in the rate equations are approximate and may lead to some inaccuracy in the absolute values of the temperatures, $T_{\max}$, of maximum ion abundances. However, the repercussions of the rate coefficient inaccuracy on $T_{\max}$ evaluation are quite moderate, since the temperature dependence of the ionization (and inner-shell excitation) rate coefficients is very steep. Thus, while an error of a factor of 5 (like by neglecting the EA processes) gives a relative shift of more than 40%, an inaccuracy of 50% in the rate coefficients would lead to a discrepancy of less than 15%.

Moreover, the aim of the present coronal balance computations is, rather, the calculation of the *relative* temperature shift due to EA, and this relative shift should not be significantly affected by the rate coefficient approximations.

The large relative shifts obtained demonstrate the relevance of EA processes in the study of ionized heavy elements in laboratory plasma, such as in tokamaks or in x-ray laser experiments.

APPENDIX A: ANALYTICAL EXPRESSION FOR THE SUBSHELL IONIZATION ENERGIES

The calculation of the ionization balance as well as the enhancement factor R due to EA processes requires the knowledge of the direct ionization rate coefficients S_r which are calculated using the Lotz formula (3). These involve the ionization energies $E_{r,s}$ for electrons in the different subshells, which are computed using the RELAC code.

The results can be conveniently represented by the following approximate analytical expression:

$$E_{r,s}=\sigma_{\mathrm{H}}^{s}(r+1)^2+A_s+B_s(r+1)+C_s(r+1)^2+D_s(r+1)^3 . \quad \text{(A1)}$$

$E_{r,s}$ is given here in eV. $\sigma_{\mathrm{H}}^{s}=R_\infty 1/n_s^2$ represents the hydrogenic ionization term expressed in eV units, where n_s is the principal quantum number of the subshell s. A_s, B_s, C_s, and D_s are constant parameters in eV for each sequence. These parameters are calculated for the binding energy of the electrons in the valence shell ($s=1$) and the next two inner subshells ($s=2,3$) using a best fit method, for all the isoelectronic sequences from Cu to Kr in the full range $40\leq Z\leq 92$. The results are given in Table IX. In fact, in the present S_r calculations the valence shell and the next three inner subshells are included. However, the contribution to the S_r total rate of the ionization of electrons in the deepest subshell is generally less than 5%. Thus the parameters for the main subshells only are given here. These parameters allow one to reproduce the energies calculated using RELAC with an accuracy of better than 0.5%, except for a few low-charge ions for which the accuracy is around 1%.

APPENDIX B: EXPRESSION FOR THE RADIATIVE RECOMBINATION RATE COEFFICIENTS

Radiative recombination is calculated using the approximate expression proposed by Von Goeler *et al.* [26]. In this approximation the recombination into excited levels is described by the hydrogenic formula [27], whereas capture into the valence shell is taken into account by introducing an effective principal quantum number. The radiative recombination rate coefficient for a recombining ion of charge $r+1$ is given by

$$\alpha_{r+1}^{R}=2.6\times 10^{-14}(r+1)^2\left[\frac{E_{\mathrm{H}}}{kT_e}\right]^{1/2}\times\left[2\Phi_{i+1}(\beta)+\frac{\mu}{i^3}ae^{a}E_1(a)\right], \quad \text{(B1)}$$

where

TABLE IX. Parameters of the analytical approximate expression for the binding energy of the electrons in the valence ($s=1$) and the two next inner subshells ($s=2,3$).

Sequence	A_1	B_1	C_1	D_1
Cu I	−37.443	14.026	−1.564[−1]	3.441[−3]
Zn I	−20.773	12.522	−7.742[−2]	2.683[−3]
Ga I	−21.430	10.761	−3.479[−2]	1.275[−3]
Ge I	−11.870	10.481	−5.512[−3]	1.033[−3]
As I	−9.6300	10.951	2.751[−3]	9.656[−4]
Se I	−7.9341	11.487	8.549[−3]	9.277[−4]
Br I	−6.5446	12.084	1.189[−2]	9.140[−4]
Kr I	−9.4329	13.293	−7.730[−3]	1.162[−3]
Sequence	A_2	B_2	C_2	D_2
Cu I	−25.655	17.291	−5.180[−4]	3.549[−4]
Zn I	−17.102	18.671	1.164[−2]	2.105[−4]
Ga I	−27.416	14.195	−1.027[−1]	2.973[−3]
Ge I	−9.5605	13.379	−5.319[−2]	2.586[−3]
As I	−4.4569	13.875	−4.101[−2]	2.520[−3]
Se I	−0.30833	14.505	−3.344[−2]	2.505[−3]
Br I	3.5823	15.208	−2.859[−2]	2.518[−3]
Kr I	1.3982	16.810	−5.794[−2]	2.923[−3]
Sequence	A_3	B_3	C_3	D_3
Cu I	22.179	27.785	−1.497[−1]	3.560[−3]
Zn I	49.785	27.549	−7.485[−2]	3.843[−3]
Ga I	−12.965	20.818	−2.303[−3]	3.318[−4]
Ge I	5.8003	21.519	2.706[−2]	5.658[−5]
As I	19.114	22.901	3.648[−2]	−4.317[−5]
Se I	29.740	24.709	3.288[−2]	−2.398[−5]
Br I	43.250	26.278	3.475[−2]	−3.922[−5]
Kr I	54.669	28.304	2.086[−2]	1.081[−4]

$$\Phi_{i+1}(\beta)=\sum_{n=i+1}^{\infty}\frac{\beta}{n^3}e^{\beta/n^2}E_1(\beta/n^2)\ , \tag{B2}$$

and

$$\beta=(r+1)^2\frac{E_{\rm H}}{kT_e}\ , \tag{B3}$$

$$a=\frac{E_r}{kT_e}\ . \tag{B4}$$

Here α^R_{r+1} is in units of $\mathrm{cm^3\,s^{-1}}$. $E_{\rm H}=13.60$ eV is the ionization energy of the hydrogen atom, and E_r $(=E_I)$ is the first ionization energy of the recombined ion r in the ground state. E_r and kT_e are in eV. n is the principal quantum number of a capturing excited level and i that of the valence shell. μ is the number of empty places in the valence shell. E_1 represents the exponential integral function.

APPENDIX C: EXPRESSION FOR THE DIELECTRONIC RECOMBINATION RATE COEFFICIENTS

The dielectronic recombination is calculated using the Burgess-Merts approximate formula [30,31]:

$$\alpha^D_{r+1}=\frac{1}{(kT_e)^{3/2}}B(r+1)\sum_k A(r+1,k)e^{-\Delta E_k/akT_e}\ , \tag{C1}$$

where

$$B(r+1)=6.5\times10^{-10}\frac{(r+1)^{1/2}(r+2)^2}{\sqrt{(r+1)^2+13.4}}\ , \tag{C2}$$

$$A(r+1,k)=\frac{f_k\sqrt{\Delta E_k}}{1+0.105(\chi_{gk})+0.015(\chi_{gk})^2}\ , \tag{C3}$$

$$a=1+0.015\frac{(r+1)^3}{(r+2)^2}\ , \tag{C4}$$

and

$$\chi_{gk}=\frac{\Delta E_k}{(r+2)E_{\rm H}}\ . \tag{C5}$$

α^D_{r+1} is in $\mathrm{cm^3\,s^{-1}}$. f_k and ΔE_k are the mean absorption oscillator strength and the average energy of the transition between the ground state and an excited configuration k of the recombining ion $r+1$. ΔE_k and kT_e are in eV. It has been noticed that the Burgess-Merts formula can overestimate the dielectronic recom-

TABLE X. Relevant quantities for use in the dielectronic recombination rate coefficient computations, for Mo, Xe, Pr, and Dy ions. ΔE_k and f_k are the average excitation energy (in eV) and the total absorption oscillator strength of the transition, respectively.

		Mo		Xe		Pr		Dy	
Sequence	Transition	ΔE_k	f_k	ΔE_k	f_k	ΔE_k	f_k	ΔE_k	f_k
Sr I	$4p^64d^2$-$4p^54d^3$	40.01	6.0	92.95	4.4	116.8	3.9	153.9	3.5
	$4d^2$-$4d5f$	38.01	0.3	220.4	0.2	323.2	0.4	493.5	0.6
Rb I	$4p^64d$-$4p^54d^2$	40.74	6.7	92.46	4.9	115.9	4.4	152.5	3.9
	$4d$-$5f$	45.95	0.1	231.7	0.1	335.4	0.2	507.7	0.3
Kr I	$3d^{10}4s^24p^6$-$3d^94s^24p^64f$	280.9	1.1	779.5	4.9	1039.8	5.7	1459.7	6.5
	$4p^6$-$4p^54d$	41.33	7.4	91.91	5.4	115.0	4.8	151.0	4.3
Br I	$3d^{10}4s^24p^5$-$3d^94s^24p^54f$	289.6	1.5	787.5	5.1	1047.5	5.9	1469.4	6.7
	$4p^5$-$4p^44d$	43.21	5.8	93.26	4.2	116.2	3.8	152.2	3.4
Se I	$3d^{10}4s^24p^4$-$3d^94s^24p^44f$	297.5	1.9	794.9	5.4	1059.8	6.2	1482.5	6.9
	$4p^4$-$4p^34d$	45.0	4.4	94.55	3.2	117.5	2.9	153.3	2.6
As I	$3d^{10}4s^24p^3$-$3d^94s^24p^34f$	304.9	2.3	803.9	5.6	1068.8	6.3	1488.0	6.9
	$4p^3$-$4p^24d$	46.67	3.1	95.82	2.3	118.6	2.0	154.4	2.5
Ge I	$3d^{10}4s^24p^2$-$3d^94s^24p^24f$	312.6	2.7	812.1	5.7	1076.5	6.4	1499.2	7.1
	$4p^2$-$4p4d$	48.3	1.9	97.05	1.4	119.7	1.3	155.4	1.2
Ga I	$3d^{10}4s^24p$-$3d^94s^24p4f$	316.4	3.0	821.5	6.1	1086.3	6.8	1514.0	7.4
	$4p$-$4d$	49.9	0.9	98.25	0.7	80.89	1.1	112.7	1.1
Zn I	$3d^{10}4s^2$-$3d^94s^24f$	327.7	3.5	830.9	6.3	1095.1	6.9	1523.7	7.5
	$4s^2$-$4s4p$	32.52	1.7	60.51	1.4	78.19	1.4	109.5	1.3
Cu I	$3d^{10}4s$-$3d^94s4f$	335.9	4.4	839.9	6.4	1104.9	7.0	1536.6	7.5
	$4s$-$4p$	31.7	0.7	65.33	0.6	83.68	0.6	115.9	0.6
Ni I	$3d^{10}$-$3d^94f$	339.6	4.4	849.2	6.5	1117.4	7.5	1545.1	7.5
Co I	$3p^63d^9$-$3p^53d^{10}$	171.6	0.2	274.6	0.2	325.4	0.2	408.8	0.2
	$3d^9$-$3d^84f$	365.0	4.5	882.5	6.1	1154.0	6.5	1588.1	6.9
Fe I	$3p^63d^8$-$3p^53d^9$	168.3	0.4	267.9	0.4	317.6	0.4	399.4	0.4
	$3d^8$-$3d^74f$	390.7	4.5	915.5	5.7	1190.0	7.5	1629.7	7.9
Mn I	$3p^63d^7$-$3p^53d^8$	164.7	0.7	261.3	0.5	309.7	0.5	390.0	0.5
	$3d^7$-$3d^64f$	418.6	3.9	948.4	5.1	1224.7	5.4	1671.9	5.6
Cr I	$3p^63d^6$-$3p^53d^7$	163.7	0.9	254.1	0.7	301.6	0.6	380.1	0.6
	$3d^6$-$3d^54f$	443.7	3.7	982.5	4.5	1261.4	1.8	1713.9	1.9

bination, usually by a factor of up to 2 [32]. To account of this overestimation, an approximation similar to that of Breton, De Michelis, and Mattioli in Ref. [20] is used: one takes $a=1$, and only one resonant $\Delta n=1$ transition and one $\Delta n=0$ transition (in those ions where such transition can be excited from the ground state) were taken into account. As suggested by Merts, Cowan, and Magee [31], the expression (C3) is valid only for $\Delta n=0$ resonant transitions; for $\Delta n=1$ transitions a modified expression is used:

$$A(r+1,k)=\frac{0.5 f_k \sqrt{\Delta E_k}}{1+0.21(\chi_{gk})+0.03(\chi_{gk})^2} . \quad \text{(C6)}$$

The list of the transitions used in the particular cases of the four elements Mo, Xe, Pr, and Dy is given in Table X. This table gives the average energy and the total absorption oscillator strength for the resonant transitions between the two configurations indicated. These values were calculated using the RELAC code.

[1] D. H. Crandall, R. A. Phaneuf, D. C. Gregory, A. M. Howald, D. W. Mueller, T. J. Morgan, G. H. Dunn, D. C. Griffin, and R. J. W. Henry, Phys. Rev. A **34**, 1757 (1986)

[2] D. C. Griffin, M. S. Pindzola, and C. Bottcher, Phys. Rev. A **36**, 3642 (1987).

[3] K. J. Reed, M. H. Chen, and D. L. Moores, Phys. Rev. A **44**, 4336 (1991).

[4] K. J. LaGattuta and Y. Hahn, Phys. Rev. A **24**, 273 (1981).

[5] J. M. Shull and M. Van Steenberg, Astrophys. J. Suppl. Ser. **48**, 95 (1982).

[6] M. Arnaud and R. Rothenflug, Astron. Astrophys. Suppl. Ser. **60**, 425 (1985).

[7] D. C. Griffin, C. Bottcher, and M. S. Pindzola, Phys. Rev. A **25**, 1374 (1982).

[8] R. D. Cowan and J. B. Mann, Astrophys. J. **232**, 940 (1979).

[9] P. Mandelbaum, M. Finkenthal, E. Meroz, J. L. Schwob, J. Oreg. W. H. Goldstein, M. Klapisch, L. Osterheld, A. Bar-Shalom, S. Lippman, L. K. Huang, and H. W. Moos, Phys. Rev. A **42**, 4412 (1990).

[10] J. Oreg, W. H. Goldstein, P. Mandelbaum, D. Mitnik, E. Meroz, J. L. Schwob, and A. Bar-Shalom, Phys. Rev. A **44**, 1741 (1991).

[11] J. Oreg, W. H. Goldstein, M. Kapisch, and A. Bar-Shalom, Phys. Rev. A **44**, 1750 (1991).

[12] D. Mitnik, P. Mandelbaum, J. L. Schwob, J. Oreg, A. Bar-Shalom, and W. H. Goldstein, in *UV and X-Ray Spectroscopy of Astrophysical and Laboratory Plasmas,* edited by E. H. Silver and S. M. Kahn (Cambridge University Press, Cambridge, England, 1993), p. 146.

[13] A. Bar-Shalom, M. Klapisch, and J. Oreg, Phys. Rev. A **38**, 1733 (1988).

[14] M. Klapisch, Comput. Phys. Commun. **2**, 239 (1971).

[15] M. Klapisch, J. L. Schwob, B.S. Fraenkel, and J. Oreg, J. Opt. Soc. Am. **67**, 148 (1977).

[16] M. H. Chen and B. Crasemann, At. Data Nucl. Data Tables **38**, 382 (1988).

[17] J. Nilsen, At. Data Nucl. Data Tables **41**, 132 (1989).

[18] *Electron Impact Ionization,* edited by T. D. Märk and G. H. Dunn (Springer-Verlag, New York, 1985), Chaps. I, II, and VIII.

[19] W. Lotz, Z. Phys. **206**, 205 (1967); **216**, 241 (1968); **232**, 101 (1970).

[20] C. Breton, C. De Michelis, and M. Mattioli, J. Quant. Spectrosc. Radiat. Transfer **19**, 367 (1978).

[21] P. Mandelbaum, J. F. Seely, A. Bar-Shalom, and M. Klapisch, Phys. Rev. A **44**, 5744 (1991).

[22] H. Van Regemorter, Astrophys. J. **136**, 906 (1962).

[23] R. V. D. R. Wooley and C. W. Allen, Mon. Not. R. Astron. Soc. **108**, 292 (1948).

[24] G. Elwert, Z. Naturforsch. **72**, 432 (1952).

[25] D. J. McLaughlin and Y. Hahn, Phys. Rev. A **43**, 1313 (1991).

[26] S. Von Goeler, W. Stodiek, H. Eubank, H. Fishman, S. Grebenshchikov, and E. Hinnov, Nucl. Fusion **15**, 301 (1975).

[27] L. Spitzer, Jr., Astrophys. J. **107**, 6 (1948); *Physics of Fully Ionized Gases,* 2nd ed. (Wiley, New York, 1962), p. 150.

[28] J. Dubau and S. Volonté, Rep. Prog. Phys. **43**, 199 (1980).

[29] Y. Hahn and K. J. LaGattuta, Phys. Rep. **166**, 195 (1988).

[30] A. Burgess, Astrophys. J. **141**, 1588 (1965).

[31] A. Merts, R. D. Cowan, and N. H. Magee, Jr., Los Alamos Scientific Laboratory Report No. LA-6220-MS (1976) (unpublished).

[32] M. H. Chen, Phys. Rev. A **34**, 1073 (1986).